Graphene based Solution Gated Field-Effect Transistors (SGFET) for Biosensors

A Thesis

Submitted to the Department of Electrical and Electronic Engineering

Of

BRAC University

By

Abdullah Hossain Sarker	17121060
Maisha Tabassum	14121062
Nafis Erfan	14121046

Supervised by
Dr. Md. Mossaddequr Rahman
Professor
Department of Electrical and Electronic Engineering
BRAC University, Dhaka

Co-Supervised by
Md. Anamul Hoque
Lecturer
Department of Electrical and Electronic Engineering
BRAC University, Dhaka

In partial fulfilment of the requirements for the degree of
Bachelor of Science in Electrical and Electronic Engineering

Spring 2018
BRAC University, Dhaka

Declaration

We hereby declare that this work titled “Graphene based Solution Gated Field-Effect Transistors (SGFET) for Biosensors” is our own work. The work has not been presented elsewhere for assessment. Materials used from sources have been properly acknowledged and referred.

Signature of
Supervisor

……
Dr. Md. Mossaddequr Rahman

Signature of
Co-Supervisor

……
Md. Anamul Hoque

Signature of
Authors

……
Abdullah Hossain Sarker

……
Maisha Tabassum

……
Nafis Erfan

Acknowledgement

To begin with, we would like to express our sincere and earnest gratitude to Almighty Allah (S.W.T) for helping us successfully complete our undergraduate thesis in Electrical and Electronics Engineering.

We want to express our sincere gratitude to our thesis Supervisor, Professor Dr. Md. Mossaddequr Rahman and Co-Supervisor, Md. Anamul Hoque, for their guidance, motivation, immense knowledge which helped us in doing this thesis. Without the help, support, feedback, encouragement and constant support of our Co-Supervisor, Md. Anamul Hoque, the research, analysis and overall the completion of our thesis could not have been possible. We would like to thank Electrical and Electronics Engineering (EEE) Department, School of Engineering and Computer Science, BRAC University, for providing us with the necessary facilities. The data we analyzed in this thesis were provided by our Co-Supervisor, which he had recorded and developed during his internship at Walter Schottky Institute, Technical University of Munich, Germany.

We would also like to thank our family and friends for their constant support and belief in us.

Abdullah Hossain Sarker,

Maisha Tabassum,

Nafis Erfan.

Dhaka, April 2018

Abstract

Graphene based SGFETs offer several advantages over other sensing devices in aqueous environment due to the exceptional properties of Graphene. Properties of Graphene such as high tunability, sensitivity, rigidity, flexibility, chemical stability and bio-inertness plays a very crucial role in biosensors by not inducing scars and damages in the surrounding tissues. Also, being only one atom thick, allows the fabrication of fully flexible high performance Graphene transistor possible. We will study the various parameters, low frequency noise characteristics in Graphene based SGFETs and observe the I-V characteristic along with the shifts of the Dirac point which will help us to identify charged membranes upon Graphene. We will be working with positively charged DOTAP lipid bilayer membrane upon Graphene due to its viability with biosensors. This will give us the basis for understanding the mechanism of charged molecules sensing using Graphene device.

Table of Contents

List of Figures

List of Tables

Nomenclature

f	Frequency
I-V	Current-Voltage Characteristics
DNA	Deoxyribonucleic Acid
2D	Two dimensional
ε_0	Dielectric constant of air
GaN	Gallium Nitride
AlGaN	Aluminum Gallium Nitride
NaCl	Sodium Chloride
Ag	Silver
AgCl	Silver Chloride
Si	Silicon
CMOS	Complementary Metal Oxide Semiconductor
V	Volts
s	Seconds
OH	Hydroxide
TFE	Tetra Fluoro Ethylene
$FeCl_3$	Iron Chloride (III)
DAQ	Data Acquisition
n_e	Number of electrons

1

Introduction

Since its discovery by Andre Geim and Kostya Novoselov at the University of Manchester in 2004, the electrically isolated graphene has gained tremendous interest due to its exceptional properties such as highly tunability, high sensitivity depending on various parameters amongst few. Also, graphene being chemically stable makes it bio-inert [1][2][3]. Along with significant application possibilities in electronics, solar cells, gas detection, DNA sequencing and many other fields, graphene is also a sensible material for Solution Gated Field-Effect Transistors (SGFETs) making it very promising for biosensors for sensing in an aqueous environment [4][5][6]. Graphene-based SGFETs offer several advantages compared to other sensing techniques in an aqueous environment as silicon-based SGFETs are not very stable in the electrolyte. Chemical properties of graphene allow the graphene transistors to be built and gated through an electrolyte. Moreover, Graphene being only one atom thick means it can be transferred to almost any arbitrary substrate which allows fabrication of fully flexible high-performance graphene transistor possible. Graphene results from sp^2 hybridized carbon atoms, whose interatomic bond is one of the strongest in nature, thus graphene shows very high rigidity, flexibility, chemical stability and capability of being unharmed in the harsh biological environment. The choice of graphene in biosensors is undoubtedly reasonable as graphene's flexibility and rigidity plays a very crucial role in biosensors by not inducing scars and damages in the surrounding tissues around the sensor device as highly rigid and sharp crystalline prostheses on biosensor devices make them unsuitable for biological environments such as human body. Electronic properties of graphene describe how graphene SGFETs show high sensitivity. It is a zero band gap semiconductor. Charge carriers close to charge neutrality point i.e. the Dirac point behave like partially relativistic particles which provide extremely high charge carrier mobility resulting in high sensitivity. Another important requirement for a good sensor is to have a low electronic noise. Reduction of noise at low frequencies (<100 KHz) is essential in order to sense for e.g. cells on top of SGFETs. $1/f$ noise, whose origin and the

microscopic mechanism is still having a controversial discussion, dominates the low-frequency noise. Graphene offers new possibilities to explore the origin of the $1/f$ noise. This implies that the low-frequency noise in SGFET can be characterized [7]. Moreover, through observing the I-V characteristic and the shifting of the Dirac point, identification of charged membrane is possible. To evaluate the electrical response of graphene to charged lipid membranes, biomimetic membranes of different charges can be assembled on graphene. Also, graphene is electrically sensitive to charge adsorption. By changing the ion concentration in analytic solution, the shift in the Dirac point can be observed and through this pH can also be determined. Thus, graphene is a very promising material for building a stable and highly sensitive sensor. As negatively charged lipid bilayer upon graphene has shown a decrease in mobility (μ) of charges by up to 25% thus positively charged DOTAP lipid bilayer upon graphene is viable for bio-sensors. With positively charged lipid bi-layer, SGFETs is known to exhibit high mobility, large transconductance, and high sensitivity. Hence our work is with positively charged DOTAP lipid bilayer membrane.

The scope of this Thesis

Graphene is a compound that is suitable for optical detection of sensitivity changes, for its chemical robustness and unique electromagnetic properties. Graphene-based sensors have already been shown to have successfully detected single-atom gas molecules and DNA detection as well as the electronic noises of the system [1][2][3].

In the prior experiment, post-fabrication of the graphene-based FET, the data regarding electrical characteristics of 32 graphene-based SGFETs in a single chip was dispensed to us, in order to be analyzed. The transistors were gated with an electrolyte solution along with a buffer solution called Phosphate-Buffered Saline (PBS). It is a water-based salt solution containing di-sodium phosphate and a buffer. The buffer helps to maintain a constant pH. Each of the transistors on the chip was characterized electrically at different electrolyte ion concentrations in a constant 5 mM PBS buffer solution, with and without a positively charged lipid bilayer called DOTAP. By varying gate-source voltage, U_{GS} and observing drain-source current, I_{DS}, whilst keeping drain-source voltage, U_{DS} constant at 0.1 Volt. Upon increasing the ion concentration of the electrolyte solution, we observed a left shift in the Fermi-Dirac point.

Upon repeating the experiment by adding DOTAP lipid bi-layer on the graphene SGFET channel, there was a further left shift of the Fermi-Dirac point. However, there was no change observed upon an increase in the ion concentration of the electrolyte solution. Charge carrier mobilities are obtained from the data obtained from the experiments conducted on the 32 transistors and a brief comparison with other work in the same field is done. Lastly, a noise analysis of the solution gated FET (SGFET) was done, in order to characterize its response to high-frequency signals. In the frequency range between 1 Hz to 10 kHz, all graphene transistors exhibited a $1/f$ type of noise. This is the $1/f$ type of noise is known as the flicker noise of the system.

The flicker noise exhibits a $1/f^{\beta}$ dependence, where the parameter β is dependent on the material and the structure of the device. During prior experiments and analysis, β was found to vary from 0.9-1.1. The noise signal, S_I was also found to be directly proportional to the square of the drain-source current, I_{DS}. The noise amplitude, A depends on the square of the transconductance, g_m. An S_I Vs f graph was plotted for three different U_{GS}: 0V (for hole carrier transport), 0.2V (close to the Dirac point) and 0.45V (for electron carrier transport). Upon analysis, it was found that at U_{GS}=0.2V, the magnitude of the noise was the lowest. This was because the transconductance is lowest at this value of U_{GS}.

The following chapter (i.e. Chapter 2) is going to present a literature review on the structural properties of graphene and Silicon based MOSFETs and how it compares to graphene-based FETs in terms of electronic characteristics along with the highlights of electronic characteristics of graphene SGFET and how it holds up against the other FETs. Also, in this chapter, we will discuss Lipids and the formation and structure of lipid membrane on graphene along with the sensing capabilities of SGFET in a different environment and bio-compatibility of lipid membrane on graphene. Chapter 3, discusses how to grow the graphene by CVD and the steps taken to fabricate the graphene SGFET. The noise measurement techniques and the setup are put forward in the second section of Chapter 3. Chapter 4 deals with the results of the conducted experiments and analysis of the data gathered, the noise measurements and their respective rationales. Chapter 5 is the final chapter of this thesis paper and it will provide a conclusion and an outlook of the entire topic.

2

Literature Review

The exceptional properties of graphene such as its chemical stability, robustness, high sensitivity, mobility, bio-inertness etc. are due to its zero bandgap 2D structure. Hence, these features of graphene in Solution Gated Field Effect Transistors (SGFETs) play an important role in sensing biological molecules and prove to be advantageous over Si SGFETs. The energy band structure of graphene is approximated by tight bonding model or first-principles calculations. In this chapter, we will review theoretical concepts of graphene and its electronic properties followed by a comparison of Graphene and Silicon based Field Effect Transistors (FETs) and SGFETs, along with their various characteristics and properties. Lastly, we have given a brief description of lipids and DOTAP lipid and its structure along with its formation on a graphene transistor as we will be working DOTAP in this thesis work.

2.1 Graphene

Graphene is a one-atom-thick layer of carbon atoms arranged in a hexagonal lattice. It can be considered as a conceptual building block for other carbon allotropes like nanotubes, Buckyballs or graphite. In fact, many of the electronic and structural properties of the latter can be derived from graphene [8]. Graphene is the first 2D crystal that was ever realized. The 2D nature of graphene gives rise to some remarkable mechanical, electronic and chemical properties. The electrical properties impressed with an intrinsic charge carrier mobility of 200,000 cm^{-2}/Vs at room temperature, highest known in any material [8]. Also, graphene is known to be the strongest material to date. The force-displacement behavior is interpreted within a framework of nonlinear elastic stress-strain response, and yields second-order and third-order elastic stiffness of 340 Newton per meter (Nm^{-1}) and 690 Nm^{-1}, respectively [9]. The breaking strength of Graphene is 42 Nm^{-1} [9]. This value represents the intrinsic strength of a defect-free sheet. These quantities correspond to Young's modulus of E = 1.0 Tera Pascal,

the third-order elastic stiffness of D = –2.0 Tera Pascal, and intrinsic strength of σ_{int} = 130 Giga Pascal, for bulk graphite [9]. Such experiments have established that graphene is the strongest material ever measured [9]**.** It is also a very good conductor of heat. The thermal conductivity of graphene is ~4000 WmK^{-1} [8] [10].

Graphene consists of a honeycomb lattice of carbon atoms. 2s, $2p_x$, and $2p_y$ orbitals hybridize in a way that each carbon atom is bonded to its three neighbors by strong sp^2 or σ bonds. The remaining p_z orbital is perpendicular to the lattice and overlaps with other p_z orbitals for forming a π bond. The p_z electrons govern the electronic transport while being delocalized throughout the crystal [10]. The 2D lattice of sp^2 hybridized carbon atoms arranged in a honeycomb lattice of graphene is shown in Figure 2.1 (a). It can be described by a triangular lattice and a two atom basis with the lattice vectors

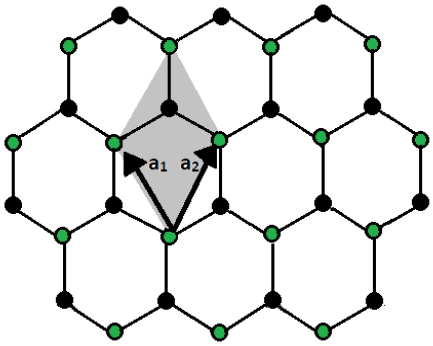

Figure 2.1 (a): The lattice vectors $\vec{a}_1$ and $\vec{a}_2$ are shown in the 2D honeycomb lattice of graphene. The gray part indicate in the above figure is the unit cell.

$$\vec{a}_1 = \frac{a}{2}(3,\sqrt{3}),\ \vec{a}_2 = \frac{a}{2}(3,-\sqrt{3}) \qquad (2.1)$$

a= 1.42Å is the distance between two neigboring carbon atoms [10].

The electronic band structure of graphene can be determined from the 2D honeycomb lattice of it. It was calculated by Wallace [10] as early as 1947 using a tight-binding approximation. The structure of a single layer of graphite was deduced, which is equivalent to graphene as a first approximation step in the investigation of the band structure of graphite.

Figure 2.1 (b) shows the electronic band structure of graphene. As there are two atoms per unit cell, there are two bands. The conduction band and the valence band touch each other at six

points in the reciprocal space. These six points are called K points, which coincide with the boundary of the first Brillouin zone. The Fermi energy lies exactly at the K points for undoped graphene since each atom contributes one electron. Therefore graphene is a so-called zero-bandgap semiconductor.

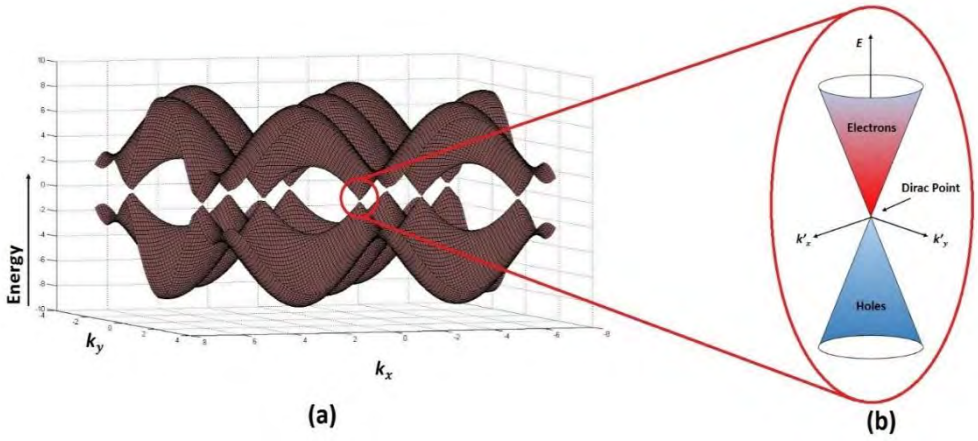

Figure 2.1 (b): (a) The band structure of graphene is shown in the reciprocal space with valence and conduction band, the valence and conduction band meet at six equivalent Dirac points. On the six corners the so-called Dirac cones can be observed (b) In the vicinity of Dirac points, the linear relation of energy dispersion is exhibited [10][11]. (Valence conduction band, Brillouin zone needs to be marked)

On each of the six corners of the Brillouin zone, the band structure reveals a linear dispersion relation which can be described by

$$E = \hbar \upsilon_f k \tag{2.2}$$

where υ_f is the Fermi velocity, with a value of υ_f ~106 m/s, k is the wave vector and $\hbar$ the reduced Planck constant [11]. The approximated value of υ_f can be calculated using tight-binding theory [10].The linear energy-momentum relation is shown in Figure 2.2 (b).

The linear energy-momentum relation results in a vanishing effective mass of the electrons and holes. Because of which the charge carriers are best described by the Dirac equation, which describes relativistic spin 1/2 particles. As a consequence, electrons and holes behave like relativistic massless particles. This explains the extraordinary high charge carrier mobilities in graphene. At room temperature, mobilities larger than $\mu = 1 \cdot 10^5$ cm^2/Vs have been reported

for graphene encapsulated in hexagonal boron-nitride. For suspended graphene, at low temperatures, mobilities of $\mu = 1 \cdot 10^6$ cm^2/Vs have been reported and at room temperature, even $\mu = 2 \cdot 10^5$ cm^2/Vs have been measured [10].

Outstanding chemical properties are also observed in graphene. It is chemically stable due to high carbon-carbon bond energy of 4.9 eV. As a result, graphene is chemically stable in aqueous electrolyte.

2.2: Field Effect Transistor (FET)

The **Field-Effect Transistor** (**FET**) is a transistor that uses an electric field to control the electrical behavior of the device. The conductivity between the drain and source terminals is controlled by an electric field in the device, which is generated by the voltage difference between the body and the gate of the device. A silicon n-type Metal-Oxide-Semiconductor Field-Effect Transistor (MOSFET) is shown in Figure 2.2 (a). The substrate is p-typed doped, two terminals labeled source (S) and drain (D) are heavily n-type doped. The region between source and drain contact is named the channel of the transistor. The third terminal labeled gate (G) which is made of metal is placed over the channel. The gate is electrically insulated by an insulating layer (typically silicon dioxide) from the transistor channel. By applying a positive voltage between the gate and the source, electrons are attracted to the substrate/insulator interface and form a conductive channel. A negative voltage depletes the channel and the transistor is switched off. Thus, the current between drain and source contacts can be controlled by the gate voltage.

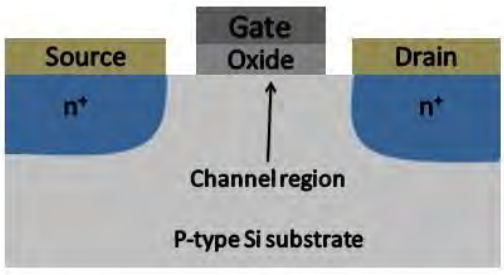

Figure2.2 (a): Cross section of an n-doped Si MOSFET

For an N-MOS, the channel is formed between source and drain terminals as the gate voltage increases beyond threshold voltage. Current will flow between source and drain due to the voltage difference between them. The magnitude of current increases linearly with increasing drain voltage till a particular drain voltage determined by the following relations:

$$U_{GS} \geq U_{th}$$

$$U_{DS} < U_{GS} - U_{th}$$

The drain to source current is represented as a linear function of gate-to-source and drain-to-source voltages. That is why the MOSFET is said to be operating in the linear region. The voltage-current relation in the linear region is given below [12] :

$$I_{DS}\,(\text{Linear}) = \mu_n\, Cox\, \frac{W}{L}[(U_{GS} - U_{th})\, U_{GS} - \frac{1}{2}U^2_{DS}] \qquad (2.3)$$

There is a particular level of voltage for drain at a particular gate and source voltage, beyond which, increasing U_{DS} seems to have no effect on the current. It is said to be saturation region when the MOSFET operates in this region for the following conditions [12]:

$$U_{GS} \geq U_{th}$$

$$U_{DS} > U_{GS} - U_{th}$$

$$I_{DS}\,(\text{Saturation}) = \frac{1}{2}\mu_n Cox\, \frac{W}{L}\,(U_{GS} - U_{th})^{\,2} \qquad (2.4)$$

Figure 2.2 (b) shows the I_{DS} vs U_{GS} curve in which the linear and saturation regions are pointed.

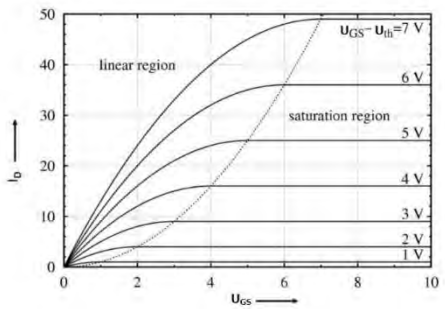

Figure 2.2 (b): MOSFET drain current vs. drain-to-source voltage for several values of the $U_{GS} - U_{th}$

The drain-source current of a MOSFET is proportional to the mobility and the interfacial capacitance:

$$I_{DS} \alpha \mu.C \quad (2.5)$$

Where $C=\varepsilon\varepsilon_0\frac{A}{d}$, with A being the channel area, ε the dielectric constant of the isolating layer and d the thickness of the isolating layer. The derivative of the drain-source current with respect to U_{GS} is the transconductance. It is an important parameter for sensors, as high transconductance allows the realization of very sensitive devices.

Traditionally, Silicon MOSFETs have been limited by Short-Channel Effects (SCE) that usually result in a reduced on-off ratio. With each generation of scaling, Dennard's scaling theory requires the depletion depth to be scaled by the same factor as the lateral dimensions; this is to maintain good gate control of the channel but requires higher channel doping; the higher doping reduces channel mobility [13][14].

In recent Si CMOS generations, Wire Capacitance (C_W), has become a major component of C (sum of device capacitance). A number of short-wire architectures have been proposed in the past; these reduce the average wire length, and thereby result in a lower average C_W, resulting in decreased capacitance.

2.3 Graphene Transistor

While Si MOSFETs are usually top-gated, early Graphene FETs (GFETs) were bottom gated. In fact, one of the main reasons for back-gating Graphene FETs are the optical visibility of Single-Layer Graphene (SLG) flakes on 300 nm of SiO_2 was [13].

Varying the gate potential changes the channel Fermi level in a Graphene FET; this, in turn, makes the graphene channel either n-type or p-type and leads to a unique current-voltage curve. The conductivity is minimum when $E_F \sim 0$ and the intrinsic carrier density of graphene is predicted to be $n_i \sim 10^{11}$ cm^{-2}. When $E_F > 0$ (i.e. $U_G < 0$), electrons are induced in the channel, leading to mostly electronic conduction. Similarly, when $E_F < 0$, the channel is in majority-hole conduction. For ideal graphene the gate voltage at which conductivity is minimum (U_{Gmin}) is zero. But fabricated samples are dependent on a number of parameters

including impurity type and density and the work function difference between graphene and the substrate [13].

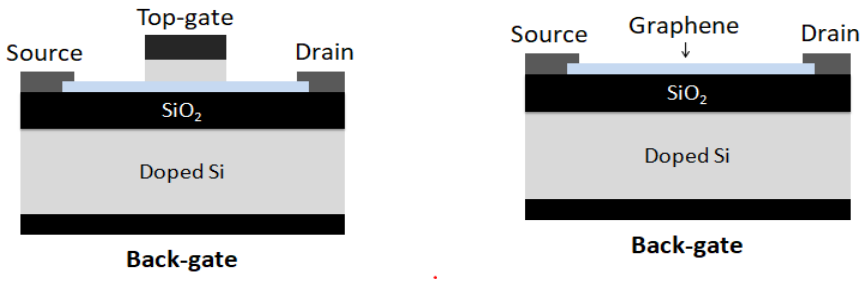

Figure 2.3: Back-gated and top-gated Graphene FETs are shown Exfoliated and CVD graphene are usually on 300nm or 90nm SiO_2 substrate on doped Si. The doped Si allows for back-gating [13].

Outstanding electronic properties are observed in graphene due to the band structure of it. Charge carriers close to the charge neutrality point which is also referred as Dirac point, behave like quasi-relativistic particles. Which largely reduces scattering and gives extremely high charge carrier mobilities. Also the fabrication of transistors without any solid dielectric is allowed by the chemical properties of graphene. Which results in giving interfacial capacitances of several μFcm^{-2}, which is almost one order of magnitude higher than for traditional semiconductors with stable dielectric. As a result, graphene shows significantly higher transconductive sensitivities than other conventional semiconductor materials used for bio-sensors [3][15].

Material	Mobility μ, (cm^2/Vs)	Capacitance C_{int}, ($\mu F/cm^2$)	Transconductance g_m (mA/V)	Biocompatibility	Flexibility
Silicon	450	0.35	0.20	0[8]	0[21]
Diamond	120	2	0.29	+[22]	-
AlGaN/GaN	1200	0.32	0.51	+[23]	-
Graphene	4000	2	5	+[24]	+[20]

Table 1: Properties of field effect transistors prepared using different material systems. Graphene gives high transconductive sensitivity due to both high charge carrier mobility and a high interfacial capacitance [3].

Table 1 shows a comparison of the relevant properties of FETs based on graphene and other commonly used semiconductor materials. Graphene-based FETs already offer advantages over the other competing technologies although graphene is still in the primary stage of research and development. In terms of biocompatibility, graphene exhibit a similar performance to diamond and AlGaN/GaN. However, to improve stability, silicon devices require additional encapsulation layers. Manufacturing flexible devices strongly deteriorates the electronic properties of silicon. The manufacturing is also not possible with single crystalline diamond or AlGaN/GaN heterostructures. On the contrary, graphene exhibits relatively high chemical stability and it is feasible to produce high quality flexible transistors [3][16][17].

Again, the subthreshold swing of graphene FET is lower than Si FET, so dynamic power dissipation is less than Si MOSFET. The minimum value of Subthreshold Swing (SS) of silicon MOSFET is 60mv/decade. Different experiments have shown that Graphene can reduce the value of SS to 40mv/decade [18]. In addition, graphene interconnects have been shown to have many advantages compared to Si CMOS interconnects, copper, including a higher current carrying capacity, lower resistivity, and smaller mutual capacitance [13][14]. So, using Graphene in FET channels can give us numerous advantages.

2.4 Graphene Solution Gated Field-Effect Transistor (SGFET)

A Solution-Gated Field-Effect (SGFET) transistor has the similar functional principle of Metal-Oxide-Semiconductor Field-Effect Transistor (MOSFET). In case of SGFET, the gate metal is replaced by a reference electrode and an electrolyte as shown in Figure 2.4 (a).

As we have discussed already that the drain-source current of a MOSFET is proportional to the mobility and the interfacial capacitance, the same goes for SGFET. And the capacitance is given by, $C=\varepsilon\varepsilon_0\frac{A}{d}$, with A being the channel area, ε the dielectric constant of the isolating layer and d the thickness of the isolating layer. One of the performance analysis parameter of the MOSFET is transconductance. Transconductance is the derivative of the drain-source current with respect to U_{GS} at a constant U_{DS}:

$$g_m = \frac{\partial I_{DS}}{\partial U_{GS}}|_{U_{DS}} \tag{2.6}$$

As high transconductance allows the realization of very sensitive devices, transconductance is an important parameter for a sensor by describing the change in I_{DS} caused by a small change in the gate voltage U_{GS}.

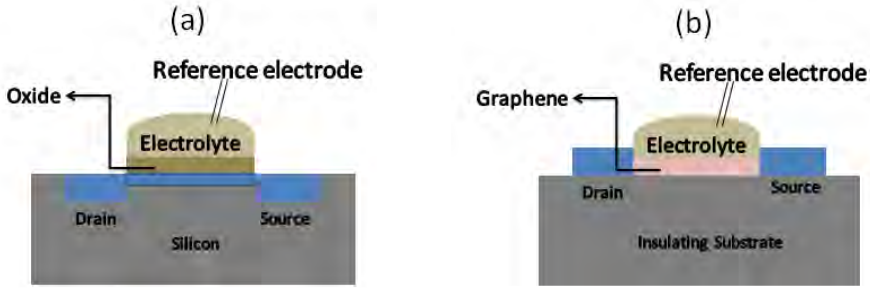

Figure 2.4 (a): (a) Silicon SGFET, (b) Graphene SGFET

The graphene layer is in direct contact with the electrolyte in Graphene SGFETs and is placed on an insulating substrate. Sapphire, Silicon dioxide, and Silicon Nitride can be used as substrates. Due to the stability of graphene in an electrolyte and its large electrochemical potential window, an insulating layer is not necessary. The graphene/electrolyte interface has a high interfacial capacitance up to 2µF/cm^2 whereas typical silicon devices have only 0.35µF/cm^2. In silicon devices, an oxide layer is always necessary to ensure their stability in an electrolyte, which decreases the capacitance of the interface. Transconductance is proportional to the mobility of charge carriers and interfacial capacitance. As a result of the high interfacial capacitance and the high mobility of charge carriers in graphene result in high transconductance. The drain and source contacts with the graphene are made with gold and this has advantages over Si CMOS because it has higher current carrying capacity, lower resistivity, and smaller mutual capacitance [10][13].

A look at the band structure of graphene and the contact to the solution is required to understand the characteristics of an SGFET. The Fermi level E_F of graphene can be shifted up or downwards by varying the gate voltage U_{GS} through the contacted electrolyte. If a gate voltage U_{GS} is applied which is lower than the Dirac voltage U_{Dirac}, the Fermi level will go beyond $_{Dirac}$. It increases the current by generating holes in the valence band. For a gate voltage of $U_{GS} = U_{Dirac}$ the Fermi level is at the Dirac point. The net charge in the graphene is zero and the point of minimum conductivity is reached. Electrons can be accumulated in the conduction band by applying a U_G higher than U_{Dirac}. By increasing gate voltage results in a further increase

of the charge carriers, which leads to an increase of the current. So depending on the position of the Fermi level relative to the Dirac point both electrons and holes can be charge carriers and thus graphene SGFETs are ambipolar devices [10][11].

In Figure 2.4 (b) I_{DS} vs. U_{GS} is plotted. The blue point demonstrates the actual current which results from the holes of the valence band, VB when the applied gate voltage is lower than the Dirac voltage. Decreasing this negative voltage applied at the gate will shift the Fermi level upwards which will decrease the number of holes in the valence band, VB and therefore the current decreases. This happens until $U_{GS} = U_{Dirac}$. After that with the increased positive voltage, the number of electrons in conduction band will increase which will result in the increased current. The redpoint demonstrates the actual current which results from the electrons of the conduction band, CB when the applied gate voltage is lower than the Dirac voltage [10][11].

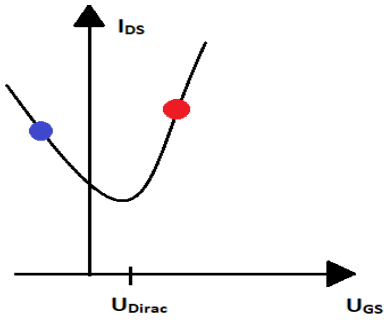

Figure 2.4 (b): I_{DS} vs. U_{GS} curve of graphene SGFET

Again in Figure 2.4 (b), I_{DS} vs. U_{DS} curve shows a characteristic V-shape. The current in graphene SGFETs can only be reduced to a minimum value it cannot be turned off completely whereas the current in Si SGFETs can be switched on and off. So graphene SGFETs give low on/off ratio compared to Si SGFETs. Though high on/off ratio is essential for digital electronics, transconductance is one of the most relevant device parameters for sensing applications [10]. Graphene-based FETs can give minimum subthreshold swing value compared to other materials. The subthreshold swing definition describes an exponential behavior of the current as a function of voltage. It is the measure of how rapidly the device switches from the OFF to the ON stage. Subthreshold swing is also the inverse of the subthreshold slope. On a graph of I_{DS} (U_{GS}) with logarithmic (base 10) axis for I_{DS} the subthreshold slope is found as the straight-line approximation of the subthreshold current,

normally expressed in units of decades/mV. Subthreshold swing is expressed in units of mV/decade.

$$\text{Subthreshold swing, SS} = \frac{dU_{GS}}{dlogI_{DS}} \tag{2.7}$$

$$\text{Subthreshold slope} = \frac{dlogI_{DS}}{dU_{GS}} \tag{2.8}$$

$$\text{And transconductance, } g_m = \frac{\partial I_{DS}}{\partial U_{GS}}|_{U_{DS}} \tag{2.9}$$

It can be said that transconductance is inversely proportional to the value of subthreshold swing. Since subthreshold of graphene is lower, the transconductance of graphene is really higher than other materials.

The features that make graphene promising for different sensing applications are summarized in the following table:

Properties	Graphene
Mobility	The mobility of both holes and electrons is very higher in graphene,~4000 cm^2/Vs
Transconductance	5 mA/V is the value of transconductance of Graphene which is really higher than the other materials
Sensitivity	Due to high transconductance, graphene shows higher sensitivity.
Flexibility	Graphene is very flexible
Chemical stability	Graphene shows superior chemical stability due to high carbon-carbon bond energy of 4.9 eV.
Capacitance	Graphene SGFETs provide large interfacial capacitance,2 $\mu F/cm^2$
Subthreshold swing	The minimum value of SS provided by Graphene is ~40mV/decade, which is lower than Si.

Table 2: The different features of graphene are stated in this table [3][18].

2.5 Lipids

Almost all living organisms have lipids or fatty acids which are one of the four major biomolecules. Lipids usually consist of two carbon chains which have varying length and degree of saturation. Glycerol structure with three OH groups works as the foundation of a lipid

and it is linked to the two fatty acid chains. Lipids have two major parts, headgroup, and tails. The headgroups are hydrophilic and tails are hydrophobic.

The headgroups can be either charged or neutral. DOTAP, 1, 2 -di-(9Z-octadecenoyl)-3-trimethylammonium propane (chloride salt), is an example for positively charged lipid. DOTAP has a headgroup which consists of glycerol and positively charged amino group [11]. In the following experiment, DOTAP, a positively charged lipid was used for the SGFET.

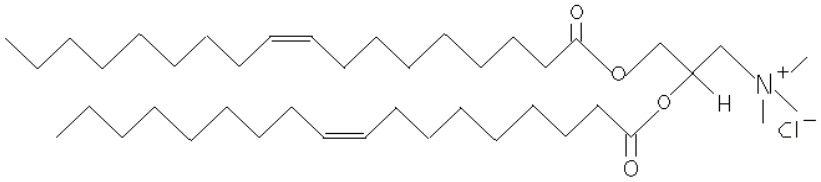

Figure 2.5 (a): Structure of DOTAP lipid: 1, 2 -di-(9Z-octadecenoyl)-3-trimethylammonium propane (chloride salt) [11]

In different environments, lipids tend to form different aggregates. The lipid bilayer is the most common one. Typically in contact with hydrophilic surfaces lipids form bilayers. Then the layers are spread on the surface and attracted by the surface via Van der Waals forces. Most of their surface facing outward consists of the hydrophilic headgroups and the tails tend to stick together. In solutions, lipids form spherical vesicles as it is the geometry with the smallest surface. In figure 2.5 (b), lipid bilayer which is typically formed at high humidity or on hydrophilic surfaces in aqueous solution is shown.

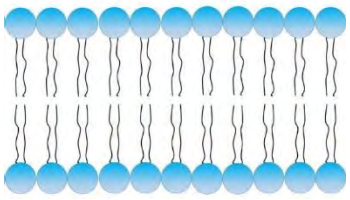

Figure 2.5 (b): lipid bilayer formed as the hydrophilic headgroups are facing outward and the hydrophobic tails are stacked together. This bilayer is typically formed on hydrophilic surfaces in aqueous solution or at high humidity [11].

2.6 Lipid Membrane Structure of Graphene

Graphene has shown fluorescence quenching properties in experiments [19]. As a result, the lipids could not be observed on top of the graphene sheet [11]. The interaction between the graphene and the lipids turned out to be much stronger [11]. Experiments have shown that lipids can form a stable monolayer when used in SGFET on top of a graphene sheet [20].

In this aggregation of form hydrophilic headgroups face to the buffer and the hydrophobic lipid tails are stick to the graphene surface. Lipids can also form a bilayer on the surface of graphene. Formation of a lipid bilayer on graphene surface was observed in the experiment that is going to be analyzed in this thesis. In the bilayer of lipid, hydrophilic headgroups are on the outward surface and hydrophobic tails are stacked together. The headgroups of one layer are stick to the graphene surface and the headgroups of another layer are faced to the buffer.

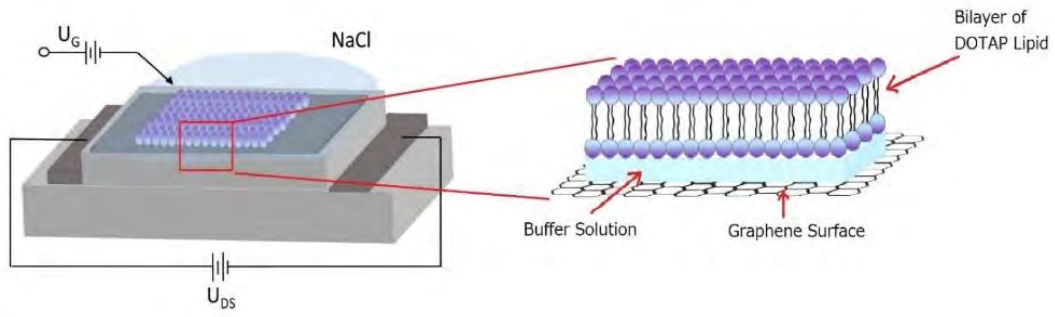

Figure 2.6: Formation of a bilayer of DOTAP lipid on top of a graphene surface using vesicle fusion technique is shown.

In the above Figure 2.6, the formation of a bilayer of DOTAP lipid on top of a graphene surface is shown. Graphene SGFET can be used in a different environment as sensing devices and the addition of lipid membrane on the graphene gives us several advantages. In the following experiment, a bilayer of DOTAP lipid was formed on top of the graphene surface using vesicle fusion technique. The lipids used in the experiment was 0.5mM/ml DOTAP in PBS buffer. The DOTAP forms bilayer to have a stable homogenous structure. The hydrophilic headgroups are in the outer part of the bilayer and the hydrophobic tail groups are stacked together to maintain stability.

2.7 Summary

The above chapter describes the general theoretical concepts relevant for this thesis work. A brief introduction of graphene and its electronic properties are discussed following with a general description of the Field Effect Transistors (FET) and Graphene FETs and a brief comparison with Silicon FETs. In addition, this chapter gives a brief description of Graphene-based Solution Gated Field Effect Transistors (SGFET), its various characteristics and a comparison with Silicon-based Solution Gated Field Effect Transistors. Later in this chapter, a short description of lipids along with DOTAP lipid and its structure along with the lipid membrane structure on a graphene transistor. In the following chapter i.e. chapter 3, the various steps to fabricate graphene SGFET is discussed, including growing of graphene using Chemical Vapor Deposition (CVD) method. Later in chapter 3, the Origin and a brief characteristic of noise in SGFET are discussed along with the setup and the technique to measure noise in SGFET.

3

Device Fabrication and Noise Measurement Technique

Geim and Novoselov first isolated Graphene in 2004 by mechanical exfoliation. They showed that Graphene could be obtained by rubbing a freshly cleaved piece of Highly Ordered Pyrolytic Graphite (HOPG) on a tape, and then transferred onto a Silicon substrate with a native oxide. This method is termed as 'Mechanical Exfoliation'. A sheet of carbon atoms i.e. graphene sheet was identified which was visible in an optical microscope due to the contrast exhibited when placed on a Si substrate with 300 nm thick SiO2 owing to the interference in the optical path upon reflection. However, for large sheets of graphene to be synthesized Chemical Vapor Deposition (CVD) method is used due to economic reasons. Graphene is only one atom thick that translates to the fact that it has the ability to be transferred to almost any substrate. This allows fabrication of fully flexible high-performance graphene transistor possible. In this chapter, we will discuss the formation of graphene sheets along with the steps required to fabricate graphene SFGET. Later in this chapter, a brief review of characteristics of noise in SGFET is done along with noise measurement technique in SGFET and its set up.

3.1 Device Fabrication Process

In this chapter, we will discuss the fabrication process of graphene-based Solution Gated Field Effect Transistors (SGFET). **Chemical Vapor Deposition (CVD)** is a much more scalable and is an efficient form of graphene production in comparison to Mechanical exfoliation and thermal decomposition. CVD is also relatively more cost-effective in producing large sheets of top-grade graphene with a high value for carrier mobility (about 4000 cm^2 V^{-1} s^{-1}) [21]. However, this wasn't always the case. Graphene grown using CVD exhibited low charge carrier mobilities compared to exfoliation methods [10]. This was due to the chemical contaminants introduced during the transfer process. The applying of mechanical stress and the

Grain boundaries of CVD grown graphene were also significant causes. But now CVD technique has been improved to overcome this limitation.

In order to grow the graphene, firstly a copper foil is mounted on a holder and taken in a glass tube. Two different approaches can be taken when using a reactor: 1) hot wall approach 2) cold wall approach. The hot wall approach can be used to maintain uniform temperatures with restively low pressure. However, it causes contamination and reaction on the walls. In the cold wall approach, there is no reaction I the walls, but the temperature is hard to maintain. Here, we have taken the hot wall approach. High temperatures and relatively low pressures are maintained in the reactor. The foil is then heated to 1000°C in an oven or a furnace also known as a Hot-wall reactor (which has an advantage of maintaining temperature uniform throughout), under the influence of 700 sccm hydrogen-argon gas mixture flow[1] as depicted in figure 3.1 (a). Maintaining the flow at this temperature for about 30 minutes etches the copper foil off dirt and copper oxide [10]. The gas flow is then changed to 70 sccm methane-argon gas mixture and 400 sccm of hydrogen-argon[2].

The methane provides the carbon source needed for the graphene formation on the copper foil. A pressure of 9 mbar is maintained. After 30 minutes of heating and allowing the graphene to grow, the copper foil is removed from the oven and is allowed to cool in the 70 sccm methane-argon[1] and 400 sccm hydrogen-argon[2] combinations [10]. The graphene obtained this way is a fairly good grade, the nature of which can be tested by Raman Spectroscopy.

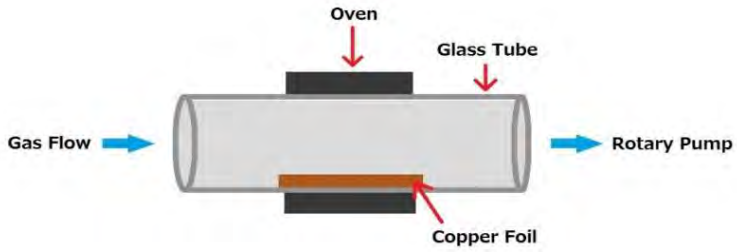

Figure 3.1 (a): Process of formation of a graphene sheet on a copper foil by Chemical Vapor Deposition, in a Hot-wall reactor (furnace) that is heated to 1000°C, under the flow of methane and hydrogen gas, which break into carbon atoms and forms thin layer of graphene [22].

[1] 14 % Hydrogen, 96% Argon, Linde AG
[2] 25% Methane and 95% Argon, Linde AG

CVD is a bottom-up approach to produce graphene. This means that the graphene that is produced on the metal sheet seeping in on the upper surface from the bottom. This phenomenon is clearly depicted in figure 3.1(b). The methane gas molecules get oxygenated (removal of hydrogen) to Carbon and they settle on the surface of the foil, under the high temperature. The carbon atoms then slowly start to seep inside the metal surface. Upon cooling, these carbon atoms resurface as either single or multiple sheets of graphene. The produced sheets can then be extracted for use [22][23].

Figure 3.1 (b): Chemical Vapor Deposition - The high temperature causes the methane to break down into carbon atoms on the surface of the metal foil sheet. These carbon seeps underneath the surface and upon cooling, these carbon atoms resurface in layers and accumulate into a single sheet(s) [21][22].

The graphene-copper stack created is then spin-coated in a photoresist called **Polymethyl 2-methyl propanoate (PMMA).** This is an organic compound with the formula $(CH_3)_2CO$**.** It provides mechanical stability to the graphene sheet. Next, the Copper layer in the stack is etched away by applying it to the Iron (III) Chloride solution. The remainder of graphene-PMMA layer is then diluted (to remove residue PMMA) and the graphene stack is fished on to a sapphire substrate. The PMMA is removed by dissolving it in a particular solvent like acetone. Other solvents like TFE, Chloroform, and Toluene can be used as alternatives. Then the photoresist upon the graphene-sapphire substrate stack is annealed away, removing any final traces of PMMA and leaving only the graphene and the sapphire substrate stack as depicted in figure 3.1 (c) [3].

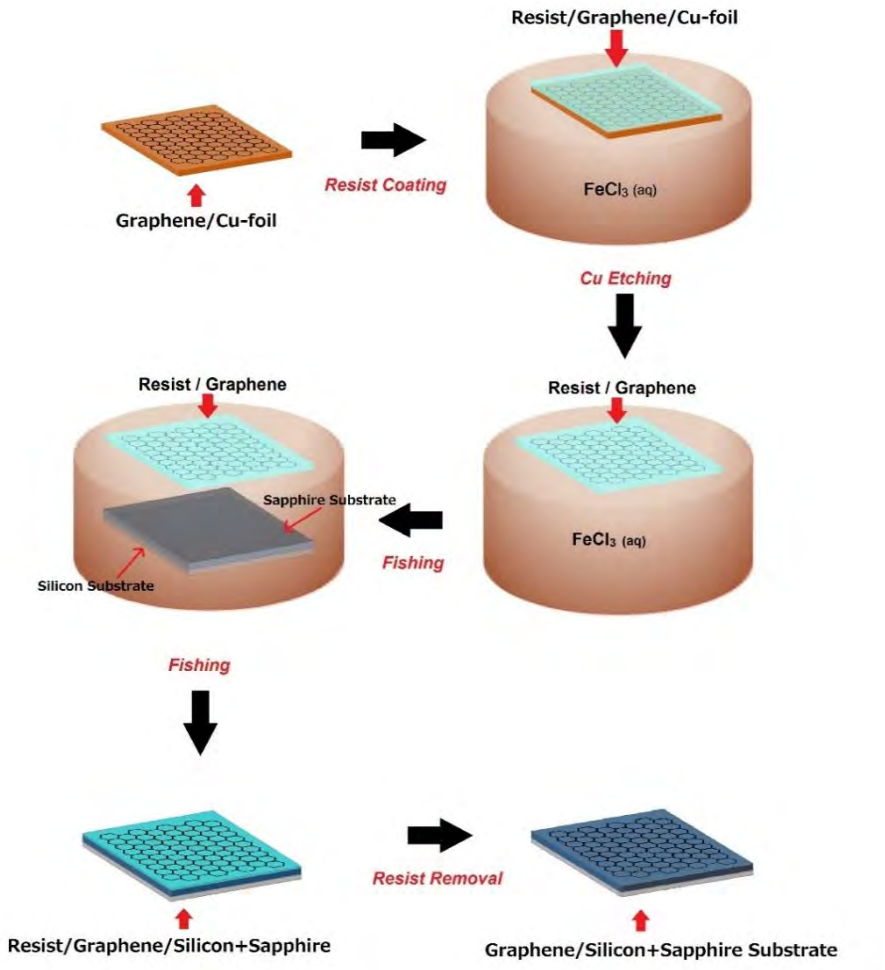

Figure 3.1 (c): Graphene-Copper stack is coated with PMMA resist and then $FeCl_3$ (aq) solution is used to dissolve copper from the stack. The resist-graphene sheet is then fished onto an isolated Silicon-Sapphire substrate stack and then the resist is removed giving us a Graphene-Silicon+Sapphire substrate stack [3].

The graphene is then patterned using optical lithography and the active region is defined by Oxygen plasma etching as depicted in figure 3.1 (d). The drain and source contacts are defined by gold evaporation technique (a method used for thin film deposition of gold) and etching any excess, using Potassium Iodide or Iodide solution. Then a photoresist called **SU8,** a commonly used epoxy-based negative photoresist is applied onto the entire upper surface of the graphene, in order to insulate the gold contacts from the electrolyte and also to keep the leakage currents to a minimum. To ensure complete coverage of the gold a small part of the graphene is also covered by the insulating photoresist [10].

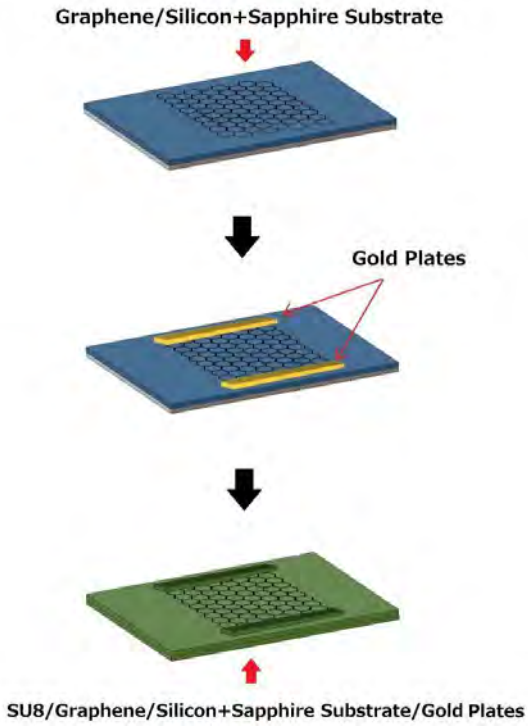

Figure 3.1 (d): Active region of the transistors first defined by etching the graphene by oxygen plasma and then by applying gold pates as contacts. Then a chemically resistive resin SU8 is applied on to the surface of the transistor so that it remains functional while using electrolytes [3].

A final annealing step is followed by the attachments of bonding wires to the chip carrier. Silicone glue is used to isolate the bond pads and wires against the electrolyte. The electrolyte is filled into a glass ring serving as an electrolyte container as depicted in figure 3.1 [10].

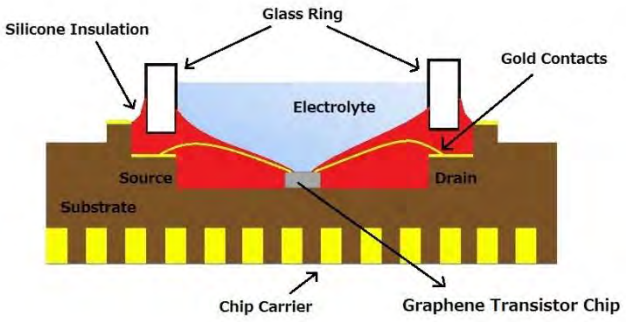

Figure 3.1 (e): The device (brown) is bonded with wire (gold lines) to a chip carrier which is then sealed with silicone glue (red) and a glass ring is mounted on top of it [10].

The transistor is developed in arrays to meet the demanded spatial resolution. A single transistor made in through this process has the dimension of 20 µm by 20 µm. A close-up of a single transistor amongst transistor array is shown in figure 3.1 (f) [3].

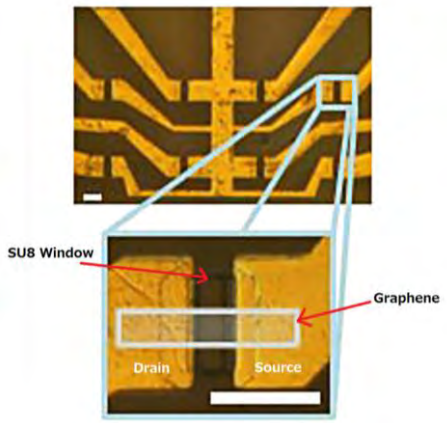

Figure 3.1 (f): Optical micrograph of a 4x4 transistor array and the isolation of a single transistor with a drain, source, graphene (white) and SU8 window (black) [3].

3.2 Noise Measurement Technique

3.2.1 Origin and Characteristics of Noise in SGFET

Noise is a random fluctuation in an electrical signal. There are various sources of such noises. A very prominent source is thermal motion. It is the (random) movement of a particle associated with the particle's thermal energy. Such a noise sometimes named: Thermal noise, Johnson noise, or Nyquist noise is the electronic noise generated by the thermal agitation of the charge carriers (usually the electrons) inside an electrical conductor at equilibrium, which happens regardless of any applied voltage. In this paper, we will analyze flicker noise which exhibits a $1/f^{\beta}$ dependence and the parameter β which varies depending on the material and the structure of device [11].

3.2.2 Noise Measurement Setup

To measure the noise affecting the SGFET, a protection mechanism must be used to prevent any other external noise source from affecting the results. This is why a Faraday Cage is used which is an enclosure used to block any external electromagnetic fields. The Noise setup i.e. the SGFET board is encased in the copper Faraday cage, and drain-source voltage U_{DS} and a gate voltage U_G is applied to the transistor. The resulting drain-source current I_{DS} is amplified with a factor of 10^6 and converted to a corresponding voltage U_{out}. The corresponding voltage of I_{DS} is filtered to ensure the Shannon-Nyquist Criterion[3] [11].

Three low-pass filters with different cut-off frequencies: f_c = 150Hz, 4 kHz and 15.9 kHz is chosen for the measurement then averaged [11]. The curves are fitted for each LPF and extended to cover the whole spectrum to exclude the effects of the high pass filter of the measurement setup in low ranges (1 - 10 Hz) and the thermal noise contribution at high frequencies. A high-pass filter with f_c = 0.53 Hz removes the DC-component of the signal. In the last step, the signal is then read out from a DAQ-Card which converts analog signals to

[3] **Shannon-Nyquist Criterion:** $f_s > 2f_{max}$. The sampling frequency f_s has to be more as the double of the highest frequency f_{max} appearing in the signal, to avoid any aliasing effect.

digital signals which can be further interpreted by the computer [11]. Then it is processed by a software that applies Fourier Transform to it and conserves the frequencies between 1 Hz-40 kHz [11]. This range is also called the frequency spectrum.

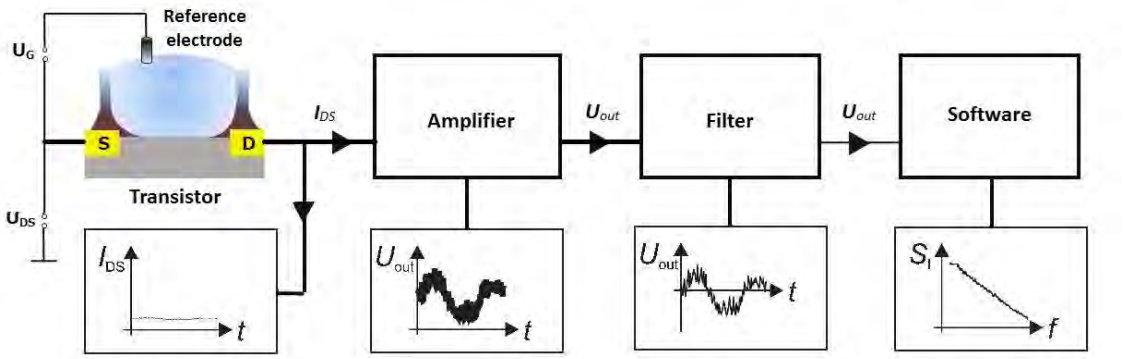

Figure 3.2.2: A Schematic view of the noise measurement technique set up. U_{DS} or U_G is applied in the DAQ-card or the accumulators. The I_{DS} signal we get is then amplified 10^6 times and converted to a corresponding voltage, U_{out}. This is then filtered using a High-Pass filter of cutoff frequency, $f_c = 0.53$ Hz and three selected different Low-Pass filters, $f_c = 150$ Hz, 4 kHz, 15.9 kHz). Lastly, the signal is read by the DAQ-card and is Fourier-transformed [11].

3.3 Summary

In this chapter, we have discussed the process of growing of graphene using Chemical Vapor Deposition (CVD) method and fabricating graphene SGFET. Next, a brief characteristic of noise in SGFET is reviewed along with the setup and the technique to measure noise in SGFET. In Chapter 4, we will analyze the data collected from the experiments conducted on the SGFET, in order to determine the electronic characteristics with and without lipid membrane and along with their comparison. The analysis of charge carrier mobilities of SGFET with and without lipids is discussed along with the cause of shift of the curve (I_{DS} vs U_{GS}) obtained from the data. Furthermore, the noise measurements taken from the experiments will be analyzed to obtain an approximate value of β, fitting parameter a, and the overall noise signal equation.

4

Electronic Characteristics of Graphene SGFETs with and without Lipid

After fabricating the graphene-based FET, we move onto the electrical characterization of the device. Each of the fabricated chip contains 32 graphene-based transistors were electrically characterized at different ion concentrations in 5mM PBS buffer solution to obtain vital information of the electronic characteristics of graphene SGFET to facilitate further experiments. In this chapter, we analyze the data obtained from the 32 transistors with and without lipid to observe the shift in Dirac point by varying electrolyte concentration from 1mM to 500mM to determine the cause behind such shifts and ion sensitivity as these help in identification of biological molecules. Also, resistances on the hole dominated the region, Dirac Point and the electron dominated region to better understand the characteristic V shape of the I_{DS} vs U_{GS} curve. Charge carrier mobilities, μ with and without lipid are determined. Also, the reason of noise signal being proportional to $1/f^{\beta}$ and its dependence on transconductance g_m is investigated as low electronic noise at high frequency is essential for a good biosensor. Later, a comparison is done with Yung Yu Wang's work and other works in the same field with our results.

4.1 Electronic Characteristics of SGFET

The transistor array is immersed in a solution containing 5mM Phosphate Buffered Saline (PBS) with an ionic strength of 100mM NaCl in order to characterize in the electrolyte. The gate voltage U_{GS} is applied between the Ag/AgCl reference electrode and the source contact of the transistors. When a voltage is applied between the drain and the source, a current I_{DS} is observed between the drain and source of the transistor. This I_{DS} current is proportional to this voltage, U_{DS}. And it can be modulated by the gate voltage, U_{GS} [3].

Out of the 32 transistors, here we have taken the best one amongst them to understand the electrical characteristics especially the current vs. voltage characteristics of a graphene SGFET. Here we can observe the change of the current I_{DS} which flows between the drain and source contact of the transistor, is due to the change of the applied gate voltage U_{GS} through the reference Ag/AgCl electrode.

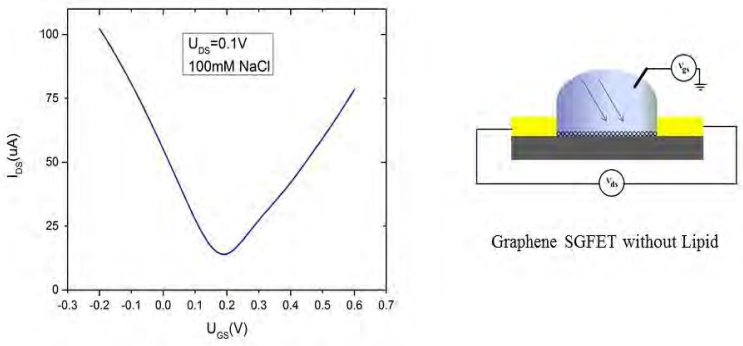

Figure 4.1.1: Current vs. voltage characteristic of graphene SGFET. The drain-source current is plotted against the gate-source voltage. The current shows a minimum value at the Dirac points and increases afar from this point. The transistor taken was characterized in 5mM PBS with an ion concentration of 100mM at U_{DS}=0.1V.

In figure 4.1.1 the current vs. voltage characteristic of graphene SGFET is shown where the current I_{DS} is plotted against the gate-source voltage U_{GS}. From the figure, it can be seen that at one specific point of voltage the current is minimum which is called the Dirac point. And the current increases continuously afar from the Dirac point on both sides. The transistor shown here has a width of 20µm and length of 20µm as well.

The following table 3 shows 3 different voltages taken from the I_{DS} vs. U_{GS} plot of the channel. One of the voltages is the voltage of the Dirac point and the corresponding drain-source current at that point of the channel. The other two voltages are from the left side of the Dirac point and the other is the right side. Here we have also calculated the resistances at these points. From the table below we can observe that the resistance is highest at the Dirac point and far from this point, the resistance keeps decreasing thus giving the characteristic curve a V shape.

	U_{GS}(V)	I_{DS}(A)	R(Ω)
Left side of Dirac Point	0.59	$8.2x10^{-5}$	1.3K
Dirac Point	0.19	$1.4x10^{-5}$	13.57K
Right side of Dirac Point	0.105	$7.54x10^{-5}$	7.8K

Table 3: Observing different U_{GS} voltages and corresponding I_{DS} and determining the resistances at those points. Resistance is highest at Dirac point and is lower at either side of Dirac point.

The observation from this table shows how the proportionality of I_{DS} and U_{DS} can be modulated by the gate voltage U_{GS}. The resistance works as the proportionality constant for the I_{DS} vs. U_{DS} curve. Since we see that the resistance is changing with the change of U_{GS}, it can be said that for different gate-source voltage the slope for the I_{DS} vs. U_{DS} will be different.

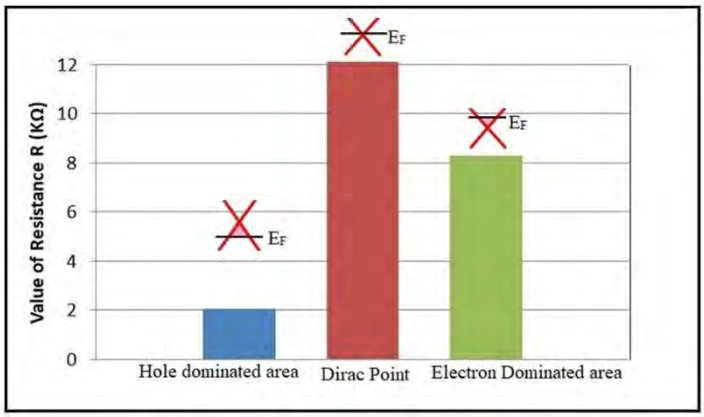

Figure 4.1.2: Resistance is highest at the Dirac point and on both the left and right side of the Dirac point, the resistance reduces significantly.

4.2 SGFETs without Lipid

Firstly, the device parameters: I_{DS}, U_{GS} and U_{DS}, were measured in neutral conditions, with standard PBS buffer solution and fixed ion concentration of 5mM. This was done in order to get the reference values for the Dirac point. The ion concentration was later varied and the changes to the I_{DS} and the reference Dirac point were observed.

In order to demonstrate the sensing applications of the devices they were investigated with liquid gating in different NaCl concentration. The transistor characteristics such as I_{DS} and U_{GS} were measured and were used to construct the characteristic I_{DS} Vs. U_{GS} curve for all the 32 transistors, as shown in figure 4.2 (a).The applied U_{DS} was kept constant at 0.1 V and all the devices were kept in 5mM PBS with the ionic strength of 100mM NaCl solution. As depicted by the curve, the transistors exhibit a 'V' shape, with a single dip in most of the devices. However, some double dips can also be observed. This can be attributed to non-uniformity in the formation of graphene, during the CVD growth, transfer process. Some uneven residuals from the fabrication process could also be responsible for such an effect, in the characteristic curve.

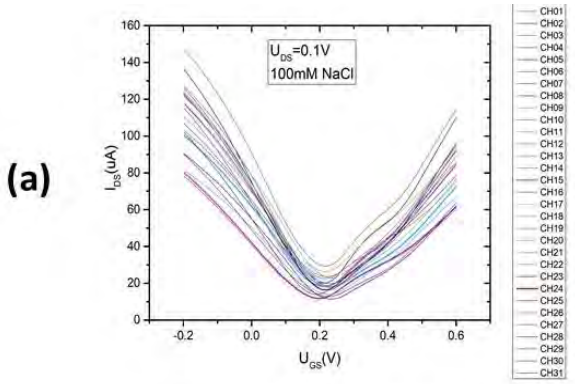

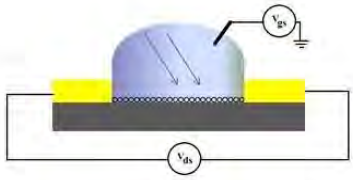

Graphene SGFET without Lipid

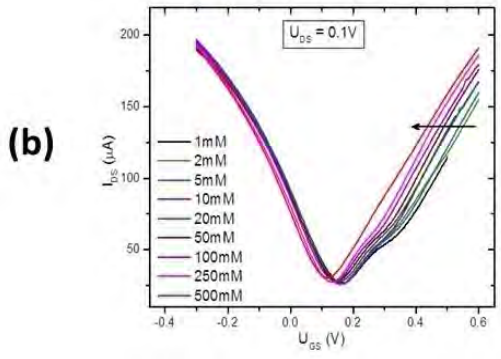

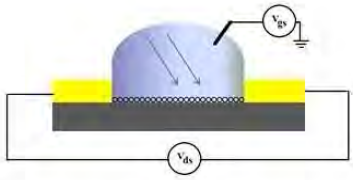

Graphene SGFET without Lipid

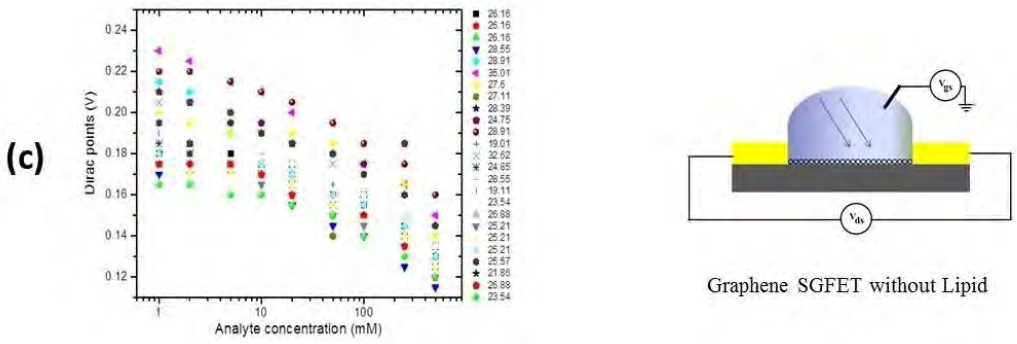

Figure 4.2: Transistor characteristics of graphene-based SGFET without lipid. (a) Current with different gate voltages for 32 transistors in 5mM PBS buffer with an ion concentration 100mM NaCl at U_{DS} = 0.1V. On the right side there is a schematic view of the device without lipid bilayer (b) Current with different gate voltages for different ion concentration, ranges from 1-500mM at U_{DS}= 0.1V. (c) Dirac points for at different molar concentration for 25 transistors. From the slope, ion sensitivity can be estimated. The ion sensitivity measured is about 25mV/decade.

Figure 4.2 (a) shows drain-source current as a function of the gate voltage in different NaCl concentrations. In the figure, the I_{DS} vs. U_{GS} characteristic curve of a single transistor, in ion concentrations ranging from 1mM to 500mM, is shown. The ion concentrations are varied in the 5mM PBS buffer solution, in order to maintain a constant pH value. The figure shows that, upon increasing NaCl ion concentration, the Dirac points shift to the left. This is depicted by the black arrow in Figure 4.2 (b). It is also intuitive that the more concentration of the ions in the solution, the greater will be the number of negative and positively charged ions. The negatively charged ion at the gate will be attracted by the holes of the positively doped graphene. The neutralizing of certain holes will cause the Dirac point to shift more towards the intrinsic case. Hence, the Dirac cone will thus be shifted to the left. This is indicating an electrostatic gating effect. The electrostatic gating effect is generated by surface potential at the graphene-liquid interface. The negative surface potential is formed when the negative surface charge which is screened by ions attracts mobile positive charges to the graphene-liquid interface [19]. These positive charges are both positive charges (holes) in the graphene and positive ions in the electrical double layer in the solution. The electrical double layer is compressed when the concentration is increased because then the ionic strength is higher. The

compressed double layer will decrease the negative surface potential. Then to compensate this negative surface potential less amount of positive gate voltage is required. Hence, the positive shift of the Dirac point becomes smaller [19]. Figure 4.2 (c) shows the Dirac points of 25 devices at different ion concentrations. The average slope of sensing ion concentration or the ion sensitivity is about 25mV/decade.

4.3 SGFET with Lipid

In the next step, lipid vesicles of 100nm diameter (in PBS buffer) were added, using vesicle fusion technique in order to have a homogeneous bilayer of lipids on graphene channel. After an incubation time of several minutes and repeated flushing with deionized water and PBS buffer, the above-mentioned parameters were measured to quantify the lipid-coated transistors. The lipids used for the experiments were 0.5mM/ml DOTAP, in PBS buffer. Similar to the first step, the ion concentration was varied and changes to the I_{DS} and the reference Dirac point were observed. It is critical for the devices to maintain both graphene's extreme sensitivity and the DOTAP lipids' chemical and electrical isolation from the electrolyte environment in order to build a sensitive and selective biosensor platform.

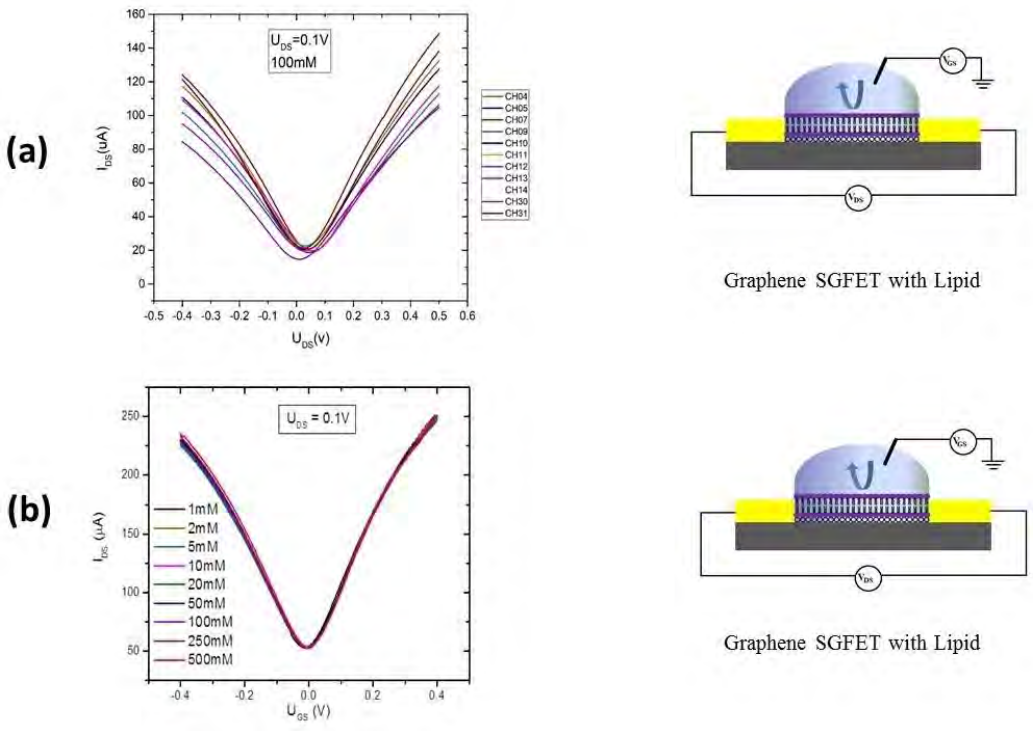

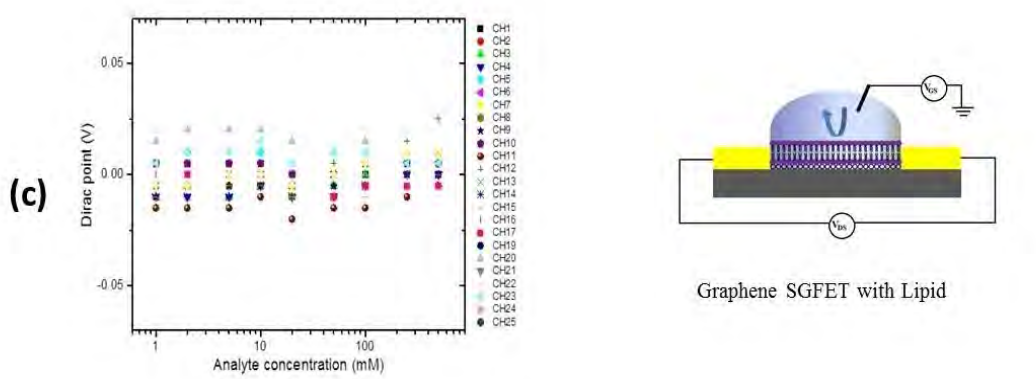

Figure 4.3: Transistor characteristics of graphene-based SGFET with lipid on top. (a) Current with different gate voltages of 11 transistors in 5mM PBS buffer with an ion concentration 100mM NaCl at U_{DS} = 0.1V. On the right side there is a schematic view of the device with lipid bilayer (b) Current with different gate voltages for different ion concentration, ranges from 1-500mM at U_{DS} = 0.1V. (c) Dirac points for at different molar concentration for 25 transistors. Unlike without lipid, there was approximately no change of Dirac points upon increasing ion concentration of the electrolyte.

The lipid has a positively charged head group. It gets physisorbed[4] on the graphene and neutralizes the surface charges, that results from adatoms[5]. Figure 4.3 (a) shows the transistor characteristics of a single device at different ion concentrations, ranging from 1 - 500mM, with U_{DS} = 0.1V. One can see that here with increasing ion concentration there is nearly no change in Dirac points.

Also, with the increased ionic strength no shift of the Dirac point is observed. This demonstrates that after the deposition of the DOTAP lipid the sensitivity of the Dirac point to NaCl concentration is completely removed. This indicates that an effective chemical and electrostatic barrier between the graphene and the electrolyte solution is created after the DOTAP lipids are formed [19].

[4] **Physisorption**, also called physical adsorption, is a process in which the electronic structure of the atom or molecule is barely perturbed upon adsorption.

[5] An **adatom** is an atom that lies on a crystal surface, and can be thought of as the opposite of a surface vacancy.

This phenomenon is termed to be the screening effect of the lipid. Here DOTAP lipids are isolating the graphene and electrolyte through screening effect. Hence, the Dirac point of the graphene is not affected anymore by the changing of concentration of the electrolyte.

Even increasing the electrolyte ion strength from 1mM to 500mM does not have a significant influence on the Dirac point of the transistors. This is due to the screening effect of the positively charged lipids. The approximate area of one Lipid is 50 $Å^2$ and with one positive charge on each lipid the surface charge density can be calculated to be $\approx 2 \times 10^{14}$ charges/cm^2 = $+3.2 \times 10^{-5}$ C/cm^2. This is up to three times higher than the surface charge of the graphene and of opposite sign to it. This indicates that the charged lipids can easily screen the graphene charges in solution. Figure 4.3 (c) depicts the Dirac points for 25 devices at different ion concentrations. For the entire chip, we observed no change of Dirac points at different ion concentrations.

4.4 Comparison of SGETs with and without Lipid

The comparison can be done between SGFETs with and without lipids by observing the shift of Dirac point of graphene. In order to study the effect of lipid on graphene channel, we have compared its electrical characterization without and with lipid, placed on top of graphene channel. Figure 4.4 (a) shows the I_{DS} with U_{GS} of the same channel with and without graphene in 1mM ion concentration with U_{DS} =0.1V. There is 200mV of a left shift of the Dirac point due to a positive head group of the lipid. Figure 4.4 (b) shows the Dirac points of the about 25 transistors in the chip with and without lipid along with cleaning the chip with a surfactant. We can see that without lipid the Dirac points are near 200mV and after adding the lipid it shifted close to 0V.

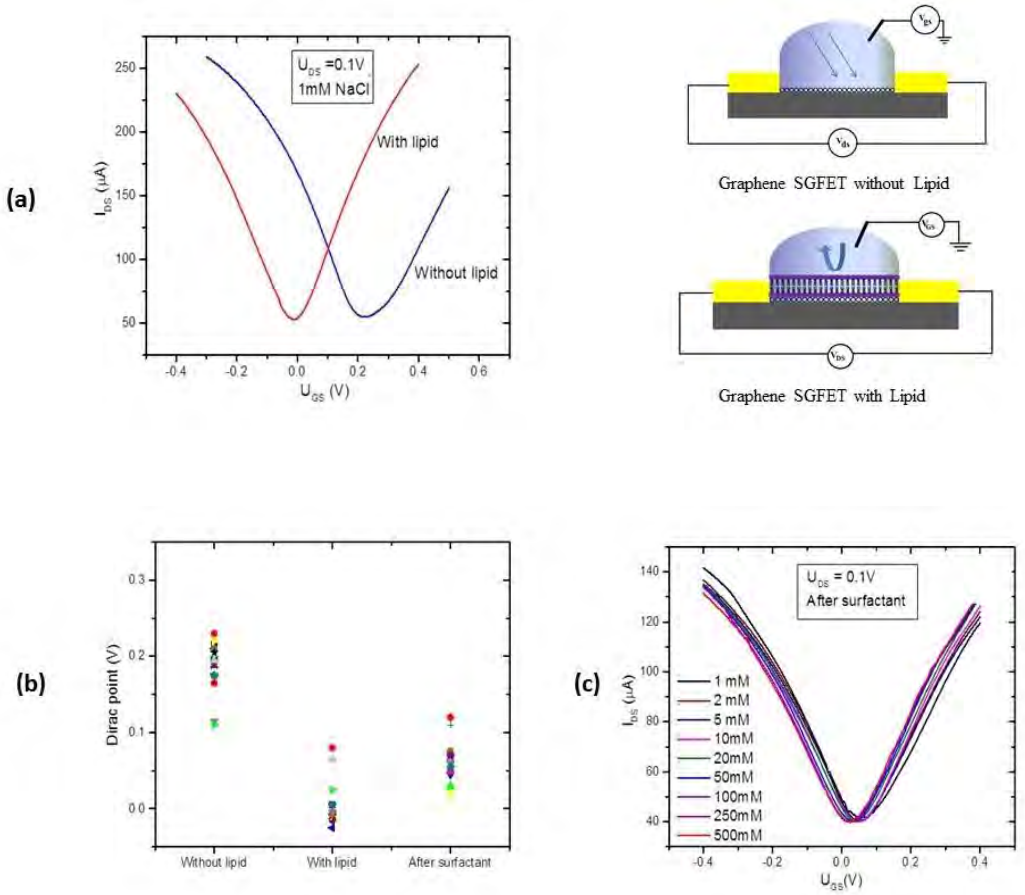

Figure 4.4: Comparison of SGFETs with and without lipid. (a) Current with gate voltages of a transistor with and without lipid. (b) Dirac points of several transistors without lipid, with lipid and after washing with the surfactant. (c) Current with gate voltages after washing the chip by surfactant at different ion concentrations.

It can be seen that there are some points, in the lipid category, which are close to 100mV. This is because the formation of the lipid bilayer on the transistor gate was not completely homogeneous. Upon cleaning the surface with surfactant and characterizing the transistors with electrical measurements once again, a shift of the Dirac points was observed, but the primary stage had not been reached, without the lipid. That indicates that the cleaning of the channel was not totally complete.

The source-drain current, I_{DS}, as a function of gate voltages in different ion concentration after adding surfactant has been shown in Figure 4.4 (c). There is a small change in I_{DS} with ion concentration. Figure 4.4 (b) shows the Dirac points of the transistor in the whole chip. The change of Dirac points with ion concentration is approximately 10mV/decade,

which is less compare to bare graphene channel (20mV/decade), shown in Figure 4.4 (b). So it can be said that the channel was not completely clean of lipids.

It is observed that a single layer of graphene field-effect transistor is sensitive to different NaCl concentrations by observing the shift of Graphene's Dirac point Figure 4.4 (a) shows drain-source current as a function of the gate voltage in different NaCl concentrations. The I_{DS}-U_{GS} curve is shifted to left while the ionic strength is increased. Whereas when graphene SGFETs are covered with DOTAP lipids, with the increased ionic strength no shift of the Dirac point is observed. Here DOTAP lipids are creating a screening effect which is isolating the graphene and electrolyte. So the graphene's Dirac point is no longer affected by the changed concentration of the electrolyte. In figure 4.4 (a), the I_{DS}-U_{GS} curve is shown when SGFET is covered with DOTAP lipids. The figure shows that there is almost no change in Dirac point of graphene with the increasing concentration of the electrolyte. So there are some significant differences in the characteristic parameters that were observed for SGFETs with and without lipids.

4.5 2nd Time Lipid Formation on SGFET

After using the DOTAP lipid for the first, we observed a left shift of 200mV in the Dirac point in the transistors. The experiment was repeated to check whether a shift can be observed again. Thus, the device was cleaned with a surfactant to remove the DOTAP bilayer and its residues. Then again DOTAP lipid was added and the experiment was repeated. After analyzing the data acquired, again a left shift of Dirac point was observed. But this time the shift of Dirac point was not identical to the shift observed during the first time as it can be seen in figure 4.5. This maybe is due to the fact that not enough time was given for the DOTAP lipid bilayer to be formed homogenously upon the graphene layer in the device.

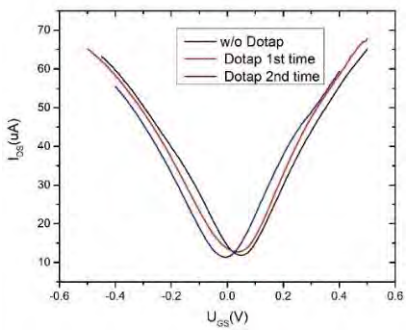

Figure 4.5: There is a difference in shift of Dirac point observed after using DOTAP for the first time and later on cleaning the device with surfactant and the shift observed after adding DOTAP lipid for the second time.

Perhaps if enough time was given for the bilayer to form, we would have observed the same amount of shift as the first time of using DOTAP. Nonetheless, the shift of Dirac point after the second time of adding DOTAP indicates the reusability of the device for sensing purposes.

4.6 Noise Measurements

To study the response of the transistor with a high-frequency signal, noise analysis of the transistor was undertaken. Figure 4.2 (a) shows the transistor behavior of the transistor in 5mM PBS buffer with U_{DS} =0.1V. The Dirac point of the transistor is close to 200 mV. Here, we have investigated the 1/*f* noise, also called the flicker noise of the system. As the name suggests, flicker noise exhibits a 1/*f* dependence and the parameter β varies depending on the material and the structure of device taken within the frequencies ranging between 1 kHz and 10 kHz.

The noise signal, $\mathbf{S_I}$ equation is given by:

$$\mathbf{S_I} = af^{\beta} \tag{4.1}$$

Where *a* and β are the fitting parameters. In our experiments, β varies from -0.9 to -1.1 on average taken from channels of 3 transistors from the array, as can be seen from Table 4:

	T1		T4		T13
U_G	β	U_G	β	U_G	β
0V	-0.89727	0V	-0.93827	0V	-0.99394
.1V	-0.91834	.1V	-0.93827	.1V	-0.84534
.2V	-0.8442	.2V	-0.91968	.2V	-0.93835
.3V	-0.83435	.3V	-1.1419	.3V	-0.84186
.4V	-1.09846	.4V	-0.95493	.4V	-0.79586
.55V	-0.92489	.55V	-0.93847	.55V	-0.93323
$\bar{\beta}$	-1.1152	$\bar{\beta}$	-0.956217	$\bar{\beta}$	-0.992895

Table 4: Average values of β obtained from experimental data by varying gate voltage U_G from 0 – 0.55V of 3 transistors 1, 4 and 13 amongst the array of transistors.

The value of β being approximately equal to -1.1 indicates that the noise signal, $\mathbf{S_I}$ is, in fact, proportional to 1/*f*. The magnitude of $\mathbf{S_I}$ depends on the square of I_{DS} and on the noise amplitude A, as shown in the following equation:

$$S_I = \frac{a}{f^{\beta}} = A.\frac{I_{DS}^2}{f^{\beta}} \tag{4.2}$$

Here, S_I is noise signal, A^2/Hz. *A* and *a* are noise amplitude and are constant. The figure, 4.6.1 (c) shows the noise signals for three different gate voltages. For, U_{GS}= 0.2V, noise amplitude (shown in red line) is lower than other values of U_{GS} because, at this voltage, transconductance g_m is the lowest.

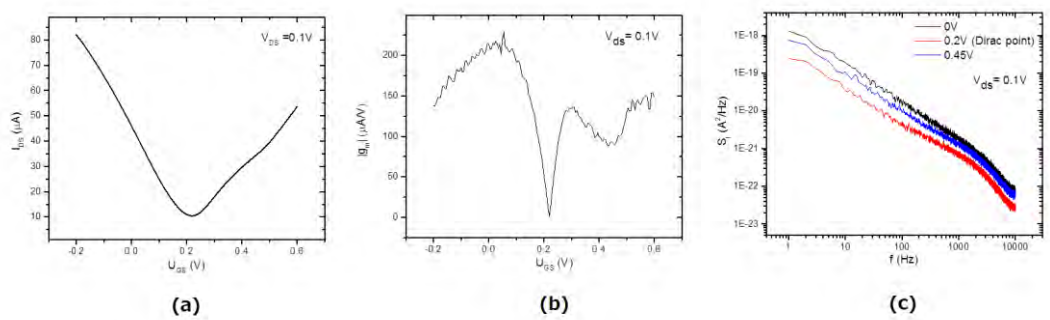

Figure 4.6.1: Noise responses of solution gated field-effect transistors. (a) Transistor characteristics of a graphene-based SGFET. (b) The transconductance of the transistor. (c) Noise responses of the transistor for three different gate voltages, 0V (hole transport), 0.2V (close to Dirac point), 0.45V (electron transport).

The noise amplitude A varies with gate voltage U_{GS} thus giving a variation in the noise signal. Various models have been proposed to explain the $1/f$ noise in graphene SGFETs. One such model which is Tersoff's model for carbon nanotube transistors [24] has been adopted by Heller for graphene SGFETs [25] to explain the dependence of noise signal amplitude, A on transconductance g_m and drain-source current I_{DS} as indicated by the equation:

$$A = S\left(\frac{g_m}{I_{DS}}\right)^2 + \alpha_S I_{DS}^2 \qquad (4.2)$$

Where S and α_S are fitting parameters for the measured noise data. This indicates the noise signal amplitude, A to be proportional to the square of transconductance, g_m. This explains the lower noise amplitude at Dirac voltage, U_{GS} = 0.2V than other U_{GS} values as shown by the red line in figure 4.6.1 (c) because the transconductance g_m is the lowest at Dirac point of the transistor.

To get the noise signal amplitude, a, each noise signal was fitted with equation (4.2) as shown in figure 4.6.2 (a) which shows us that the noise amplitude is lower near the Dirac point. Wiener-Khinchin theorem given by the equation: $\overline{x_n^2(t)} = \int_0^{3\,kHz} S_I(f)df$, was used to get the RMS value of the noise signal, U_{RMS} as shown in figure 4.6.2 (b). At Dirac point, U_{RMS} is higher because at this point the conduction is at the lowest as the number of holes and electrons are equal and the Fermi level is at the mid-point from conduction and valence band.

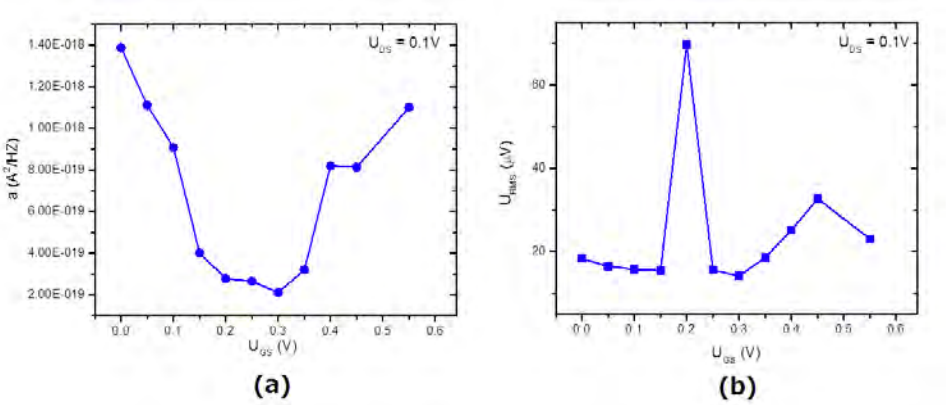

Figure 4.6.2: Noise responses from the theoretical function. (a) The slope of the noise at different U_{GS}. (b) Noise amplitude at different U_{GS}.

4.7 Charge Carrier Mobility with and without Lipid

Graphene has the capability to outnumber other semiconductors used for making different sensing devices such as biosensors. And one of the major reasons behind this is the extremely high charge carrier mobilities [3] are found in graphene [10]. During the fabrication process, the mobility of the charge carriers might be affected [10]. There are several other factors that affect graphene's mobility. There is also an influence of charged lipids on the graphene's charge carrier mobilities [26]. Thus, we will compare the mobilities in neutral condition i.e. without lipid and in charged condition i.e. with lipid.

The field effect mobility is determined by the following equation:

$$\mu = \frac{L}{WC_g V_{DS}} \cdot \frac{\Delta I_{DS}}{\Delta V_{GS}} \tag{4.3}$$

Where L and W are the channel length and width respectively. For our work, the channel length and width were taken 20µm each. C_{int} is the interfacial capacitance of graphene/electrolyte interface [19] [27]. The interfacial capacitance is given by the series connection of the quantum capacitance C_Q and the double layer capacitance C_{dl}:

$$c_{int} = \left(\frac{1}{C_{dl}} + \frac{1}{C_Q}\right)^{-1} \tag{4.4}$$

The double layer capacitance dominates C_{int} away from the Dirac point due to the large quantum capacitance. The smaller quantum capacitance dominates the interfacial capacitance in the vicinity of the Dirac point.

In order to obtain the slopes from I_{DS} vs. U_{GS}, we have observed the curves for both with and without DOTAP lipid on the top of the graphene SGFET at an ion concentration of 100mM and U_{DS}= 0.1V.

4.7.1 Charge Carrier Mobility without Lipid

In Figure 4.7.1, drain-source current with different gate voltages is observed in PBS of pH 7 and 100mM NaCl at U_{DS} = 0.1V. This characteristic was measured in the neutral condition of the graphene i.e. without lipid.

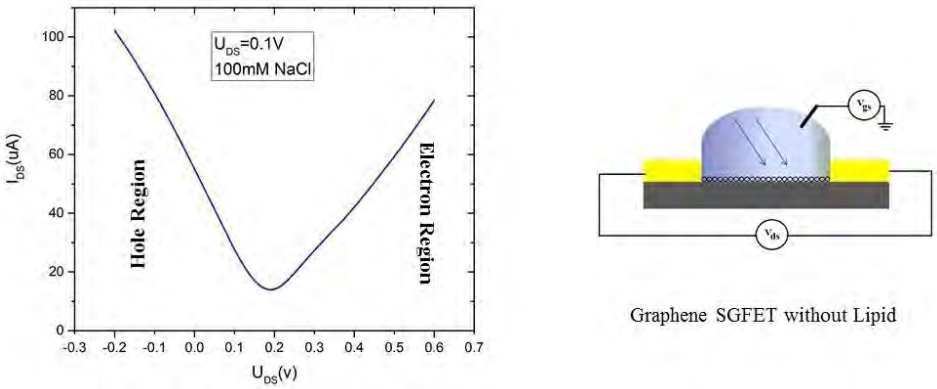

Figure 4.7.1: The I_{DS} vs. U_{GS} characteristics of graphene FET were observed in 5mM PBS at pH 7 with 100 mM NaCl. In this setup, the graphene SGFET was without lipid.

From figure 4.7.1, the slope was first taken at the left side (hole dominated region) of the curve i.e. the left of the Dirac point so as to get the mobility of holes. The slope obtained was to be -2.71x10^{-4} i.e. $\frac{\Delta I_{DS}}{\Delta V_{GS}}$ =-2.71x10^{-4}. The negative sign indicates it to be a downward slope.

Since we are calculating the slope afar from the Dirac point, the double layer capacitance dominates C_{int} and we have calculated the mobility using an interfacial capacitance, C_{int} = 2μF/cm^2 [10][28]. By applying these values to equation 4.4 we get the liquid gate hole mobility, μ_h to be 1355 cm^2/Vs.

The right (electron dominated) side from the Dirac point is an electron dominated area. So from this region, we can obtain the mobility of electrons. From figure 4.7.1, we take the slope at the right side of the Dirac point to be 1.54×10^{-4} i.e. $\frac{\Delta I_{DS}}{\Delta V_{GS}} = 1.54 \times 10^{-4}$.

Applying the obtained slope and interfacial capacitance, $C_{int} = 2\mu F/cm^2$ in equation 4.4, we get the liquid gate electron mobility, μ_e to be 770 cm^2/Vs.

4.7.2 Charge Carrier Mobility with Lipid

In Figure 4.7.2, drain-source current with different gate voltages are observed in PBS of pH 7 and 100mM NaCl at $U_{DS} = 0.1V$ This characteristic curve was obtained after the transistor was coated with lipid. The lipid used for the experiment was 0.5mM/ml DOTAP in PBS buffer.

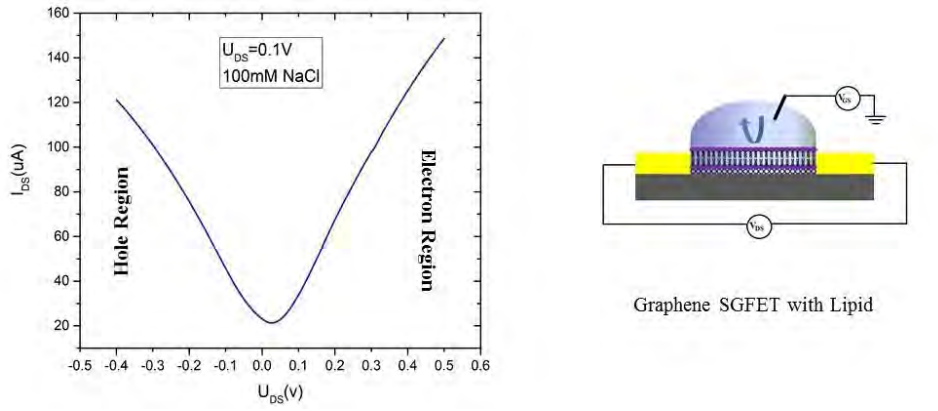

Figure 4.7.2: The I_{DS} vs. U_{GS} characteristics of graphene FET were observed in 5mM PBS at pH 7 with 100mM NaCl. This measurement was taken after formation of a lipid bilayer on top of graphene in the SGFET.

From figure 4.7.2, the slope obtained at the left (hole dominated region) side of the Dirac point was to be -2.81×10^{-4} i.e. $\frac{\Delta I_{DS}}{\Delta V_{GS}} = -2.81 \times 10^{-4}$.

Thus, applying the slope and $C_{int} = 2\mu F/cm^2$ in equation 4.4, we get the liquid gate hole mobility, μ_h to be 1405 cm^2/Vs.

The slope obtained from the right (electron dominated) side of the Dirac point is 3.28×10^{-4} i.e. $\frac{\Delta I_{DS}}{\Delta V_{GS}} = 3.28 \times 10^{-4}$.

Applying the above-obtained slope and interfacial capacitance, C_{int} = 2μF/cm^2 in equation 4.4, we get the liquid gate electron mobility, μ_e to be 1640 cm^2/Vs.

It can be clearly seen that the mobility of the charge carriers has increased after the formation of a lipid bilayer on top of graphene. The reason behind this is because of the screening effect we have talked about earlier. Due to the screening effect, the scattering rate, τ^{-1} decreases which in turn increases scattering time, τ. As scattering time, τ is directly proportional to the conductivity, σ increases as it can be seen by the equation:

$$\sigma = (\frac{e^2}{h})(\frac{2E_F\tau}{\hbar}) \quad (4.5)$$

where e is the electron charge, h is the Planck constant and E_F is the chemical potential [26].

Thus, conductivity, σ being directly proportional to mobility, μ results in increased mobility as evident by the equation [26]:

$$\mu = \frac{\sigma}{n_e} \quad (4.6)$$

Hence we get increased mobility of charge carriers in graphene-based SGFET with lipid compared to graphene SGFET without lipid.

SGFET	**Charge Carrier Mobility, μ_h (Holes)**	**Charge carrier mobility, μ_e (Electrons)**
w/o DOTAP	1355	770
w DOTAP	1405	1640

Table 5: Charge carrier mobility (holes and electrons) of graphene-based SGFET.

4.8 Comparison with other Works

We have come across other works similar to our thesis. In the other works, they too have deduced the influence of the lipid membranes on top of graphene as well as in neutral condition i.e. without lipid membrane as well as have obtained the reference values of different parameters. Now we will compare and contrast our work with the work done by Yung Yu Wang in his doctoral thesis and other groups.

4.8.1 Shift of Dirac Point for SGFET with Lipid

Figure 4.4 (a) shows the I_{DS} vs. U_{DS} of the same channel with and without lipid. The transistor array is immersed in a solution which contains 5mM Phosphate Buffered Saline (PBS) with an ionic strength of 1mM NaCl with U_{DS}=0.1V. In this case, after adding the positively charged DOTAP lipids there is a 200 mV left shift of the Dirac point. It is due to the positive head group of the lipid.

In Yung Yu Wang's work, the shift in Dirac point observed is less. In his work after adding the SLBs and the formation of the supported lipid bilayer, there is a shift in the Dirac point. The Dirac point shift of approximately 160 mV after the graphene is covered with SLBs was observed compared to the shift of 200 mV of the Dirac point of this thesis work [19].

Charged Membranes	The shift of the Dirac point (mV)
DOTAP Lipid (Positive)	200
SLBs of Yung Yu Wang's Work (Positive)	160

Table 6: The effect of different lipid charges on the Dirac point of the graphene [15].

4.8.2 Shift of Dirac Point for Different Concentrations of Electrolyte of SGFETs without Lipid

In our work, we have seen that with the increasing concentration of NaCl, the Dirac point of the graphene SGFET shifts to the left. With the increased ionic strength less amount of positive voltage is required to get the Dirac point [19]. After observing I_{DS} of a single channel with different gate voltages, U_{GS}, in various concentration of the electrolyte ranging from 1mM to 500mM, the left shift of the Dirac point was confirmed. The ion concentrations were increased in 5mM PBS to maintain the constant pH of the solution.

In Figure 4.2 (b), I_{DS} of a single transistor is plotted against different gate voltages in various ion concentrations. The black arrow indicates the left shift of the Dirac points for increasing concentration. Dirac points of 25 devices at different ion concentrations are shown in Figure 4.2 (c). By considering the average slope it can be seen that sensing of ion concentration is about 25mV/decade.

In Yung Yu Wang's work, there is a similar type of left shift of the Dirac points observed with the increase of ion concentration. He observed a shift of the I_{DS}-U_{GS} curves due to change in concentration, U_{shift} with respect to the 1 M KCl, as a function of the KCl electrolyte concentration [19]. The drain-source current, I_{DS} vs. liquid gate voltage U_{GS} characteristics of graphene FET were observed in 0.1mM phosphate buffer at pH 7 with 10 mM KCl, 100 mM KCl, and 1 M KCl and three curves for 3 different concentrations of the electrolyte were obtained. In his work, sensing of ion concentration is about 50mV/decade.

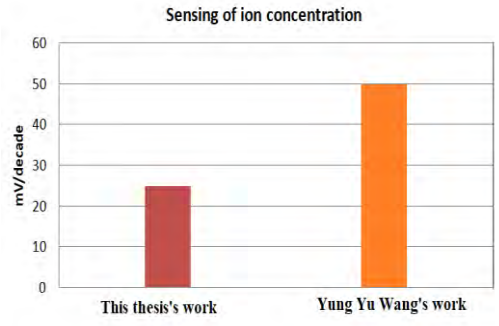

Figure 4.8.2: Showing the amount of sensitivity to the change of ion concentration observed in the two works.

When sensing of ion concentration is referred as mV/decade, it denotes that if the concentration is increased 10 times, the shift of the Dirac point will be that particular amount of mV. Both our work and Yung Yu Wang's have shown sensitivity to the ion concentration of the electrolyte. We have found 25mV/decade sensitivity of ion concentration for our work whereas Yung Yu Wang's work has observed 50mV/decade ion sensitivity.

4.8.3 Charge Carrier Mobilities for SGFETs without and with Lipid

We have calculated the charge carrier mobilities of the Graphene SGFET and we have observed that the mobilities have been increased after formation of lipid bilayers on top of graphene SGFET. The lipids used for the experiment was 0.5mM/ml DOTAP in PBS buffer.

Another group [26] has also measured electronic properties of graphene after adsorption of a charged lipid bilayer on the surface. They too have calculated the mobilities of charge carriers in neutral condition as well as in charged condition. For positively changed membrane they have used a positively charged lipid composition: DOPC/DOTAP (2:1). Almost 207 cm^2/Vs decrements of mobilities were observed after the addition of lipid [26].

The discussed work in this thesis has shown an increment of charge carrier mobilities upon formation of DOTAP lipid bilayers. On the other hand, the other group above found their mobilities to be declining as the effect of the positively charged membrane on top of graphene. Both cases have shown the influence of the lipids on the mobilities of charge carriers.

4.9 Summary

In this chapter, we analyzed the various data obtained from the experiments conducted on the SGFETs with 5mM Phosphate Buffered Saline (PBS) solution at its gate along with NaCl electrolyte at various ionic strength in order to determine the electronic characteristics and shifts in Dirac point by changing electrolyte concentration, with and without DOTAP lipid membrane. We have observed that without lipid the Dirac points were near 200mV and after adding the DOTAP lipid it shifted close to 0V and no shift observed even after increasing the electrolyte concentration. This was concluded to be due to the screening effect which isolates the graphene and electrolyte. The resistance was determined from either side of the Dirac point

with the highest being at the Dirac point and a decreasing trend in both the left (hole dominated) side and the right (electron dominated) side to explain the characteristic V shape of the curve (I_{DS} v U_{GS}) obtained in graphene SGFETs. Also, DOTAP lipid was used the 2nd time after cleaning with surfactant and the shift of Dirac point was not identical to the shift observed during the first time but almost close. This might be due to the fact that not enough time was given for the bilayer to form homogenously. A brief comparison of our work with Yung Yu Wang's doctoral thesis was in the same field was done and his work's ion sensitivity was found to be of 50mV/decade compared to ours at 25mV/decade. Charge carrier mobilities, μ with and without lipid were determined with hole mobility, μ_h = 1355 cm^2/Vs and electron mobility, μ_e = 770 cm^2/Vs without lipid and hole mobility, μ_h = 1405 cm^2/Vs and electron mobility, μ_e = 1640 cm^2/Vs with lipid a rather increase in mobility in comparison. Whereas, other works have shown a decrease in mobility after adding lipid. Also, we have discussed the reason of noise signal being proportional to $1/f^{\beta}$ and its dependence on transconductance g_m. The noise signal was found to be the lowest at Dirac point as the transconductance as well as conductance is lowest at the Dirac voltage.

`

5

Conclusion

To summarize our work, we have discussed the theoretical concepts relevant of our work such as graphene, its electronic characteristics, and its various exceptional properties in order to justify the use of graphene over silicon for SGFTEs for biological molecules detection. A review of Field Effect Transistors (FETs) such as Silicon based n-type Metal Oxide Semiconductor Field-Effect Transistor (MOSFETs) and Graphene transistors were done to compare their electronic characteristics such as charge carrier mobility (μ), interfacial capacitance (C_{int}), transconductance and their biocompatibility to show the advantages of Graphene transistors over Silicon or other FETs. The various properties and characteristics of Graphene-based Solution Gated Field Effect Transistors (SGFETs) were discussed such as its ambipolarity, transconductance, subthreshold swing, and subthreshold slope etc. A brief review of lipids in general along with DOTAP lipid's structure and its structural formation on a graphene transistor were discussed and depicted. An in-depth process of growing of graphene sheets over copper using Chemical Vapor Deposition (CVD) method is explained and depicted along with the step by step actions required to fabricate graphene SGFET. A brief characteristic of noise and its origin in SGFETs is discussed along with the measurement noise technique in SGFET and its set up. In the later chapter, we have determined the electronic characteristics and shifts in Dirac point by changing electrolyte concentration, with and without DOTAP lipid membrane with 5mM Phosphate Buffered Saline (PBS) solution at its gate along with NaCl electrolyte. Dirac points were near 200mV without lipid was observed and later after adding the DOTAP lipid, the shifted was close to 0V. No further shifts were observed even after increasing the electrolyte concentration be due to the screening effect which isolates the graphene and electrolyte. Resistances at the Dirac point and at both the left (hole dominated) side and the right (electron dominated) side were determined with the highest being at the Dirac

point and a decreasing trend in both side which explain the characteristic V shape of the curve (I_{DS} v U_{GS}) obtained in graphene-based SGFETs. 2nd-time use of DOTAP lipid was done after cleaning the device with surfactant to remove the first DOTAP bilayer formed on the device and the shift of Dirac point observed was very much like the shift of the first use of DOTAP but almost close. The reason behind this might be the fact that not enough time was given for the homogeneous formation of bilayer. The observation of shift the 2nd time proved the reusability of the device for future detections. Later, a brief comparison of our thesis work with the doctoral thesis of Yung Yu Wang and other works which are in the vicinity of our field of work was done. Ion sensitivity in Yung Yu Wang's work was found to be of 50mV/decade contrast to ours at only 25mV/decade. Charge carrier mobilities, μ with and without lipid were obtained and it was found that the mobilities of device seems to increase in contrast to other works where mobilities have in fact shown to decrease after adding lipid. A discussion and a conclusion was drawn that noise signal is proportional to $1/f^{\beta}$ as β values obtained was approximately equal to -1.1. The dependence of noise signal amplitude on transconductance g_m was deduced explain the noise signal amplitude being the lowest at Dirac point as we see the transconductance as well as conductance is lowest at the Dirac voltage.

Extensive work on this research will give us, with a certain degree of accuracy, the possibility of identification of unknown charged biological compounds using graphene devices. This could be done by comparison to the existing database of biological compounds. A potentially technologically important application of graphene is in areas such as DNA sequencing, biomarker assays for cancer detection and other protein sensing applications. Presently used FETs, for the same purpose have quite a few inherent drawbacks such as lack of stability in the extreme biological environments being a glaring disadvantage. The lack of stability means the FET ceases to function normally after a while and must be therefore be removed or replaced. Thus, it is a major challenge to develop sensors from a chemically stable material which exhibits good electronic properties and at the same time allowing fabrication of small, flexible bio-sensors compatible in a biological environment [3]. Furthermore, with a better understanding of the noise characteristics, it will be possible to achieve a more stable and accurate detection of the source signals, in terms of sensing biological molecules.

Bibliography

[1] Ang, P. K., Chen, W., Wee, A. T., & Loh, K. P. (2008). Solution-Gated Epitaxial Graphene as pH Sensor. *Journal of the American Chemical, 130*, 14392-14393.

[2] Dong, X., Shi, Y., Huang, W., Chen, P., & Li, L.-J. (2010). Electrical Detection of DNA Hybridization with Single-Base Specificity Using Transistors Based on CVD-Grown Graphene Sheets. *Advanced Materials, 22*(14), 1649-1653.

[3] Hess, L. H., Seifert, M., & Garrido, J. A. (2013). Graphene transistors for bioelectronics. *Proceedings of the IEEE, 101*(7), 1780-1792.

[4] Lee, C., Wei, X., Kysar, J. W., Hone, J. (2008). *Measurement of the elastic properties and intrinsic strength of monolayer graphene.* Columbia University, New York, Department of Mechanical Engineering. doi:10.1126/science.1157996

[5] Neto, A. C., Guinea, F., Peres, N., Novoselov, K., & Geim, A. (2009). The electronic properties of graphene. *Review of Modern Physics, 81*(109).

[6] Schneider, G. F., Kowalczyk, S. W., Calado, V. E., Pandraud, G., Zandbergen, H. W., Vandersypen, L. M., Dekker, C. (2010). *DNA translocation through graphene nanopores.* Kavli Institute of Nanoscience. doi:10.1021/nl102069z.

[7] Balandin, A. A. (2013). Low-frequency 1/f noise in graphene devices. *Nature nanotechnology, 8*(8), 549.

[8] Sagar, A. S. (2011). *Garphene-based Field-Effect Transistors.* École polytechnique fédérale de Lausanne.

[9] Lee, C., Wei1, X., & Kysar, J. W. (2008). Measurement of the Elastic Properties and Intrinsic Strength of Monolayer Graphene. *Science, 321*(5887), 385-388. doi:10.1126/science.1157996

[10] Blaschke, B. M. (2012). *Graphene Solution-Gated Field-Effect Transistors.* Walter Schottky Institut, Zentralinstitut der Technischen Universitat Munchen, Physik Department.

[11] Prexl, M. L. (2013). *Low-frequency noise of graphene solution-gated field-effect transistors.* Walter Schottky Institut, Zentralinstitut der Technischen Universitat Munchen, Physik Department.

[12] Pucknell, D. A., & Eshragian, K. (1994). *Basic VLSI Design* (3 ed.)

[13] Raghu Murali. (2012). Graphene transistors. *Graphene Nanoelectronics: From materials to Circuits.*

[14] Schwierz, F. (2013). Graphene transistors: Status, Prospects, and Problems. *Proceedings of the IEEE, 101*, 1567.

[15] Geim , A., & Novoselov, K. (2007). The rise of graphene. *Nature Materials, 6*(3), 183–191.

[16] Eda, G., Fanchini, G., & Chhowalla, M. (2008). Large-area ultrathin films of reduced graphene oxide as a transparent and flexible electronic material. *Nature Nanotechnology, 3*(4), 270–274.

[17] Kim, K., Zhao, Y., Jang, H., Lee, S., & Kim, J. (2009). Large-scale pattern growth of graphene films for stretchable transparent electrodes. *Nature, 57*(7230), 706–710.

[18] Tian, H., Tan, Z., Wu, C., Wang, X., Mohammad, M. A., Xie, D. Ren, T.-L. (2014). Novel Field-Effect Schottky Barrier Transistors Based on Graphene-MoS2 Heterojunctions. *Scientific Reports, 4*(5951). doi:10.1038/srep05951

[19] Wang, Y. Y. (2014). Graphene Based Transistors and Supported Lipid Bilayer. *University Of California, Irvine.*

[20] Holler, S. (2014). *Lipid Membranes on Sensing Surfaces Studied by X-Ray Reflectometry.*

[21] N. Petrone, C. R. Dean, I. Meric, A. M. van der Zande, P. Y. Huang, L. Wang, D. Muller, K. L. Shepard, and J. Hone.(2012) Chemical Vapor Deposition-Derived

Graphene with Electrical Performance of Exfoliated Graphene. *Nano Letters, American Chemical Society Publications 12*, 2751–2756.

[22] Li, X., Cai, W., An, J., Kim, S., Nah, J., Yang, D., …R, R. S. (2009). Large-Area Synthesis of High-Quality and Uniform Graphene Films on Copper Foils. *Science, 324*(5932), 1312-1314. doi:10.1126/science.1171245

[23] Sun, J., Cole, M. T., Lindvall, N., Teo , K. B., & Yurgens, A. (2012). Noncatalytic chemical vapor deposition of graphene on high-temperature substrates for transparent electrodes. *Applied Physics Letters, 100*(2). doi:10.1063/1.3675632

[24] J. Tersoff. (2007). Low-frequency noise in nanoscale ballistic transistors. *Nano Letters, American Chemical Society Publications, 7*, 194.

[25] I. Heller, S. Chatoor, J. Maennik, M. A. G. Zevenbergen, J. B. Oostinga, A. F. Morpurgo, C. Dekker and S. G. Lemay. (2010). Charge noise in graphene transistors. *Nano Letters, American Chemical Society Publications, 10*, 1563.

[26] Ang, P. K., Jaiswal, M., Lim, C. Y., Wang, Y., Sankaran, J., Li, A., . . . Loh, K. (2010). A Bioelectronic Platform Using a Graphene - Lipid Bilayer Interface. *ACS Nano, 4*(12), 7387–7394.

[27] Xia, J., Chen, F., Li, J., & Tao, N. (2009). Measurement of the quantum capacitance. *Nature Nanotechnology, 4*, 505–509. doi:10.1038/nnano.2009.177

[28] Hess, L., Hauf, M., Seifert, M., Speck, F., Seyller, T., Stutzmann, M., . . . Garrido, J. (2011). High-transconductance graphene solution-gated field effect transistors. *Applied Physics Letters, 99*(3). doi:10.1063/1.3614445

[29] Nomura, K.; MacDonald, A. H. Quantum Hall Ferromagnetism in Graphene. *Phys. Rev. Lett.* 2006, *96*, 256602.